



## RESEARCH ARTICLE

10.1029/2022JD036992

### Key Points:

- Model uncertainty contributes half of the total uncertainty in the projected strength of the Northern winter stratospheric polar vortex
- Uncertainty in the projected polar vortex strength is linked to uncertainty in projected regional surface temperature and precipitation
- Most climate models project an eastward shift of the Northern winter stratospheric polar vortex

### Supporting Information:

Supporting Information may be found in the online version of this article.

### Correspondence to:

A. Y. Karpechko,  
[alexey.karpechko@fmi.fi](mailto:alexey.karpechko@fmi.fi)











### Citation:

Karpechko, A. Y., Afargan-Gerstman, H., Butler, A. H., Domeisen, D. I. V., Kretschmer, M., Lawrence, Z., et al. (2022). Northern hemisphere stratosphere-troposphere circulation change in CMIP6 models: 1. Inter-model spread and scenario sensitivity. *Journal of Geophysical Research: Atmospheres*, 127, e2022JD036992. <https://doi.org/10.1029/2022JD036992>

Received 22 APR 2022

Accepted 25 AUG 2022

# Northern Hemisphere Stratosphere-Troposphere Circulation Change in CMIP6 Models: 1. Inter-Model Spread and Scenario Sensitivity

Alexey Yu. Karpechko<sup>1</sup> , Hilla Afargan-Gerstman<sup>2</sup> , Amy H. Butler<sup>3</sup> , Daniela I. V. Domeisen<sup>2,4</sup> , Marlene Kretschmer<sup>5</sup> , Zachary Lawrence<sup>6,7</sup> , Elisa Manzini<sup>8</sup> , Michael Sigmund<sup>9</sup> , Isla R. Simpson<sup>10</sup> , and Zheng Wu<sup>2</sup> 

<sup>1</sup>Finnish Meteorological Institute, Helsinki, Finland, <sup>2</sup>Institute for Atmospheric and Climate Science, ETH Zürich, Zürich, Switzerland, <sup>3</sup>National Oceanic and Atmospheric Administration (NOAA) Chemical Sciences Laboratory, Boulder, CO, USA, <sup>4</sup>University of Lausanne, Lausanne, Switzerland, <sup>5</sup>Department of Meteorology, University of Reading, Reading, UK, <sup>6</sup>Cooperative Institute for Research in Environmental Sciences, University of Colorado, Boulder, CO, USA, <sup>7</sup>National Oceanic and Atmospheric Administration (NOAA) Physical Sciences Laboratory, Boulder, CO, USA, <sup>8</sup>Max-Planck-Institut für Meteorologie, Hamburg, Germany, <sup>9</sup>Canadian Centre for Climate Modelling and Analysis, Environment and Climate Change Canada, Victoria, BC, Canada, <sup>10</sup>Climate and Global Dynamics Laboratory, National Center for Atmospheric Research, Boulder, CO, USA

**Abstract** Projected changes in the Northern Hemisphere stratospheric polar vortex are analyzed using Climate Model Intercomparison Project Phase 6 experiments. Previous studies showed that projections of the wintertime zonally averaged polar vortex strength diverge widely between climate models with no agreement on the sign of change, and that this uncertainty contributes to the regional climate change uncertainty. Here, we show that there remains large uncertainty in the projected strength of the polar vortex in experiments with global warming levels ranging from moderate (SSP245 runs) to large (Abrupt-4xCO<sub>2</sub> runs), and that the uncertainty maximizes in winter. Partitioning of the uncertainty in wintertime polar vortex strength projections reveals that, by the end of the 21st century, model uncertainty contributes half of the total uncertainty, with scenario uncertainty contributing only 10%. Regression analysis shows that up to 20% of the intermodel spread in projected precipitation over the Iberian Peninsula and northwestern US, and 20%–30% in near-surface temperature over western US and northern Eurasian, can be associated with the spread in vortex strength projections after accounting for global warming. While changes in the magnitude and sign of the zonally averaged vortex strength are uncertain, most models (>95%) predict an eastward shift of the vortex by 8°–20° degrees in longitude relative to its historical location with the magnitude of the shift increasing for larger global warming levels. There is less agreement across models on a latitudinal shift, whose direction and magnitude correlate with changes in the zonally averaged vortex strength so that vortex weakening/strengthening corresponds to a southward/poleward shift.

**Plain Language Summary** Previous studies showed that changes in the strength of the winds in the Northern Hemisphere wintertime stratosphere, the so-called polar vortex, can affect near-surface winds and precipitation on various timescales. However, climate models do not agree on whether the polar vortex will weaken or strengthen during the 21st century. Here, we use Climate Model Intercomparison Project Phase 6 experiments to better understand how the polar vortex will respond to future greenhouse gas emissions. We show that half of the uncertainty in the vortex strength projections by the end of the 21st century is due to climate model errors (model uncertainty). We show that the uncertainty in the vortex strength projections is linked to the uncertainty in projected precipitation over the Iberian Peninsula and northwestern US and projected near-surface temperature over the western US and northern Eurasia. Most models predict an eastward shift of the vortex relative to its historical location but we do not detect any influence of the vortex longitudinal shift on surface precipitation and temperatures. There is less agreement across models on a latitudinal shift, whose direction and magnitude correlate with changes in the vortex strength so that vortex weakening/strengthening corresponds to a southward/poleward shift of the vortex.

© 2022. The Authors.

This is an open access article under the terms of the [Creative Commons Attribution License](https://creativecommons.org/licenses/by/4.0/), which permits use, distribution and reproduction in any medium, provided the original work is properly cited.

## 1. Introduction

Stratosphere-troposphere coupling is an important source of surface climate variability and change from sub-seasonal to centennial timescales (see Kidston et al., 2015 for a review). It has been proposed and demonstrated that the projected changes in the strength of the Northern Hemisphere stratospheric polar vortex, the wintertime circumpolar westerly winds spanning the stratosphere north of  $\sim 50^\circ\text{N}$ , affect the climate change response of the Northern Annular Mode (NAM) and associated precipitation and windiness patterns, in particular over Europe (Karpechko & Manzini, 2012; Manzini et al., 2014; Oudar et al., 2020; Scaife et al., 2012; Shindell et al., 1999; Sigmond et al., 2004; Simpson et al., 2018; Zappa & Shepherd, 2017). Simpson et al. (2018) demonstrated that the difference in wintertime Mediterranean precipitation projections between models on opposite ends of the model spectrum of polar vortex change was on the order of 10% of the present day precipitation climatology. Understanding potential changes in the stratosphere in response to anthropogenic global warming is therefore of importance for understanding future changes in regional surface climate.

The stratosphere cools in response to increased greenhouse gas (GHG) concentrations, a thermodynamic fingerprint of global climate change (Manabe & Wetherald, 1975). At the same time, tropospheric warming affects the generation (e.g., Stephenson & Held, 1993) and propagation (e.g., Shepherd & McLandress, 2011; Sigmond & Scinocca, 2010) of atmospheric planetary and gravity waves. Wave dissipation in the stratosphere leads to complex nonlinear wave—mean flow interactions so that the net effect of the projected dynamical changes on the polar vortex can only be predicted using numerical modeling. Vertical and horizontal resolution of the climate models, as well as parameterizations of radiative processes, orographic and non-orographic gravity waves all can affect the polar vortex response to anthropogenic global warming in the models (Hardiman et al., 2012; Karpechko & Manzini, 2012; Sigmond & Scinocca, 2010).

Analysis of the models participating in the Climate Model Intercomparison Project 5 (CMIP5) revealed large uncertainty, even in the sign of the zonally averaged polar vortex strength response to increased GHGs (Manzini et al., 2014; Simpson et al., 2018; Wu et al., 2019). Nearly half of the CMIP5 models had model lids above the stratopause (1 hPa) aiming to fully resolve stratospheric dynamics. On average, these so-called “high-top” models better represented stratospheric variability and stratosphere-troposphere coupling in comparison to the “low-top” models that underestimated stratospheric variability and produced too short-lived anomalies in the Northern Annular Mode (Charlton-Perez et al., 2013; Hardiman et al., 2012). However, no significant difference in the polar vortex response to climate change between high top and low top models was found (Manzini et al., 2014; Simpson et al., 2018) suggesting that only improving numerical resolution in the stratosphere is not sufficient to constrain the polar vortex response to climate change. Similarly, large uncertainty in the magnitude and sign of the polar vortex response was found in the Climate Model Intercomparison Project 6 (CMIP6) models (Ayarzagüena et al., 2020; Rao & Garfinkel, 2021) and across chemistry-climate models that include ozone-climate interactions (Ayarzagüena et al., 2018).

Several studies have proposed explanations for the divergent stratospheric projections, linking it to spread in the amount of planetary wave activity propagating from the troposphere (Karpechko & Manzini, 2017), in the wave refraction properties of the basic states (Sigmond & Scinocca, 2010), and in the evolution of Barents-Kara Seas ice loss across models, which can affect the upward propagating planetary wave activity (Kretschmer et al., 2020; Manzini et al., 2018). However, Wu et al. (2019) found that only 27% of the CMIP5 spread is related to the amount of planetary wave activity dissipated in the polar stratosphere.

The lack of model agreement in the polar vortex response exemplifies the limited understanding of the atmospheric circulation response to anthropogenic forcing (Shepherd, 2014). Given the significant contribution of the uncertainty in polar vortex strength to regional climate change uncertainty (e.g., Simpson et al., 2018; Zappa & Shepherd, 2017), understanding the polar vortex response to global warming and narrowing down its uncertainty is a challenge that the scientific community has to address.

In this study, we investigate the polar vortex response using simulations by CMIP6 models. We progress beyond earlier studies on this topic in several ways. First, the sensitivity of the stratospheric zonal wind response to the respective emission scenario, both Shared Socioeconomic Pathways (SSP) and simplified scenarios, is analyzed in all seasons (Section 3.1). Hence, we expand on previous studies, which focused on the response in the strongest emission scenario, such as RCP8.5, and the winter season. Second, separate contributions of various sources of the uncertainty—internal variability, model uncertainty, and scenario uncertainty—are quantified (Section 3.2).

Third, a non-zonal component of the stratospheric response is considered (Section 3.3). Matsumura et al. (2021) reported a robust asymmetry in the stratospheric temperature response between American (warming) and Eurasian (cooling) sectors across CMIP5 simulations. Here, motivated by their work, we extend their analysis by examining both the longitudinal and latitudinal shifts of the polar vortex using elliptical diagnostics (Mitchell et al., 2011), as well as their impact on surface climate (Section 3.4). The methods and data used for the analysis are described in Section 2.

## 2. Data and Methods

### 2.1. CMIP Data Sets

We use data from 55 CMIP6 models listed in Table S1 in Supporting Information S1. Data from seven experiments (Historical, SSP245, SSP370, SSP585, piControl, Abrupt-4xCO<sub>2</sub>, and 1pctCO<sub>2</sub>) are used. Note that not every model performed all these experiments. Table S2 in Supporting Information S1 shows that 53% of the analyzed CMIP6 models are high-top models (model lid above 1 hPa), which is a small increase with respect to CMIP5 which has 44% high-top models (Table S3 in Supporting Information S1).

Two models (CanESM5-CanOE and MCM-UA-1-0) provided data for some of the above experiments but were not included in the analysis. CanESM5-CanOE is the same model as CanESM5 except for a different ocean biogeochemistry module that does not feedback onto the physical ocean model and, therefore, results are identical to the equivalent members of CanESM5 from the perspective of dynamical changes in the atmosphere. MCM-UA-1-0 is from a much older generation of climate models than other CMIP6 models and it has a model top at 15 hPa so it is not expected to have realistic stratospheric variability. For comparison with previous studies, we also consider the CMIP5 RCP8.5 scenario for some parts of the analysis. Table S3 in Supporting Information S1 lists CMIP5 models and number of realizations used.

We diagnose the polar vortex strength response using 10-hPa zonal mean zonal winds averaged over 60°–75°N ( $U_{10}$ ), following Simpson et al. (2018) and Wu et al. (2019). This index covers the region where the intermodel spread in zonal mean zonal wind change maximizes (Simpson et al., 2018). The climate change response is defined as a mean difference between a period in the future and a period in the past. For idealized emission scenarios abrupt-4xCO<sub>2</sub> and 1pctCO<sub>2</sub>, the difference is calculated between years 100–149 of these experiments and all years in piControl unless stated otherwise. For SSP and RCP8.5 scenarios, the difference is calculated between years 2070–2099 and years 1980–2009 of the corresponding historical simulations. Only those historical simulations that have a corresponding future scenario simulation are considered. Some historical simulations were continued for one scenario but not for the others. In such cases, model historical ensembles differ between the scenarios. Note that most of the CMIP5 historical simulations end in the year 2005; therefore, years 2006–2009 from RCP8.5 were added to the historical simulations when calculating the baseline climatology for consistency with the CMIP6 experiments. Both idealized and SSP scenarios are considered when we analyze changes in the polar vortex, while the uncertainty partitioning (Section 3.2) and sensitivity of surface response to the polar vortex response (Section 3.4) are only based on the SSP scenarios.

Multimodel mean results are obtained by first calculating ensemble mean diagnostics for individual models and then averaging across models. Thus, each model has an equal contribution to the multimodel ensemble means regardless of the number of realizations in each model.

### 2.2. Uncertainty Partitioning

Hawkins and Sutton (2009) considered the uncertainty of climate projections by a multimodel ensemble and proposed an approach to separate the total uncertainty ( $T$ ) in the response of a climate indicator into components due to internal variability ( $I$ ), scenario uncertainty ( $S$ ), and model uncertainty. Here, we apply a similar approach to analyze the uncertainty in the  $U_{10}$  response ( $\Delta U_{10}$ ) across CMIP6 models. The analysis of the uncertainty follows the approach by Yip et al. (2011) who considered the model uncertainty as consisting of two components—uncertainty independent of scenario ( $M$ ) and uncertainty dependent on scenario, or the model-scenario interaction uncertainty ( $D$ ). The original equations used by Yip et al. (2011) are modified here to account for the different number of realizations between models and scenarios

$$I(t) = \frac{1}{N_{tot}} \cdot \sum_{s=1}^{N_s} \sum_{m=1}^{N_m} \sum_{r=0}^{N_r(s,m)} [u(s, m, r, t) - \bar{u}(s, m, :, t)]^2 \quad (1)$$

$$S(t) = \frac{1}{N_{tot}} \cdot \sum_{s=1}^{N_s} N_{rs}(s) \cdot [\bar{u}(s, :, :, t) - \bar{u}(:, :, :, t)]^2 \quad (2)$$

$$M(t) = \frac{1}{N_{tot}} \cdot \sum_{m=1}^{N_m} N_{rm}(m) \cdot [\bar{u}(:, m, :, t) - \bar{u}(:, :, :, t)]^2 \quad (3)$$

$$D(t) = \frac{1}{N_{tot}} \cdot \sum_{s=1}^{N_s} \sum_{m=1}^{N_m} N_r(s, m) \cdot [\bar{u}(s, m, :, t) + \bar{u}(:, :, :, t) - \bar{u}(s, :, :, t) - \bar{u}(:, m, :, t)]^2 \quad (4)$$

$$T(t) = \frac{1}{N_{tot}} \cdot \sum_{s=1}^{N_s} \sum_{m=1}^{N_m} \sum_{r=0}^{N_r(s,m)} [u(s, m, r, t) - \bar{u}(:, :, :, t)]^2 \quad (5)$$

$$T(t) = I(t) + S(t) + M(t) + D(t) \quad (6)$$

Here,  $u(s, m, r, t)$  is the change of the quantity of interest (in our case 30-year mean  $U_{10}$ ) with respect to the reference period for scenario  $s$ , model  $m$ , realization  $r$ , and year  $t$ .  $\bar{u}(:)$  is the mean change in  $u$  averaged across the corresponding dimensions denoted by  $(:)$ .  $N_{tot}$  is the total number of realizations across all models and scenarios,  $N_m$  is the number of models for which scenario realizations are available,  $N_s$  is the number of scenarios,  $N_r(s, m)$  is the number of realizations by model  $m$  in scenario  $s$ ,  $N_{rm}$  is the total number of realizations by a model, and  $N_{rs}$  is the total number of realizations by all models in a scenario. In this study, we limit the analysis to the three SSP emission scenarios (SSP245, SSP370, and SSP585) because unlike idealized scenarios they reflect plausible future projections. Therefore, the number of scenarios,  $N_s$ , is 3, the number of models,  $N_m$ , is 47, and the number of realizations,  $N_{tot}$ , is 606.

Since some models provide a few members, their forced response may not be well separated from internal variability (Lehner et al., 2020). We partly address this issue in a sensitivity analysis where we only use models that provide at least five ensemble members (see Section 3.3).

### 2.3. Elliptical Diagnostics of the Polar Vortex

Introduced by Waugh (1997) and Mitchell et al. (2011) and modified for use with geopotential height by Seviour et al. (2013), elliptical diagnostics allow the center of the polar vortex to be located. The method by Seviour et al. (2013) defines the vortex edge using the value of the 10-hPa zonal mean geopotential height ( $Z_{10}$ ) at 60°N. Relying on predefined geopotential height values can potentially lead to biases when applied to data affected by trends such as in the climate model projections analyzed here. Instead, we define the polar vortex edge as the  $Z_{10}$  contour that corresponds to the geopotential height value at the largest absolute value of the negative gradient of geopotential height in the equivalent latitude (EqL) space (Butchart & Remsberg, 1986), requiring that this negative gradient should fall between 45° and 80° EqL. Our assumption is that trends such as stratospheric cooling that affect  $Z_{10}$  values do not as strongly affect height gradients. Since the potential vorticity needed to define EqL is not available for climate model simulations,  $Z_{10}$  was used instead because on a hemisphere it has a similar dependence on geographical latitude as potential vorticity, albeit with the opposite sign. The results presented in Section 3.3 are based on the method outlined above using monthly mean  $Z_{10}$  fields, but we confirmed that using the zonal mean geopotential height at 60°N to define the vortex edge as in Seviour et al. (2013) gives similar results.

### 2.4. Surface Response Analysis

Several studies have previously quantified the surface response to stratospheric forcing based on a regression analysis (Manzini et al., 2014; Oudar et al., 2020; Simpson et al., 2018; Zappa & Shepherd, 2017). Here, we adopt a similar regression approach given by

$$\Delta X(\lambda, \phi, m, s) = a(\lambda, \phi, s) + b(\lambda, \phi, s) \times \Delta Y(m, s) + \epsilon(\lambda, \phi, m, s) \quad (7)$$

where  $\Delta X(\lambda, \phi, m, s)$  is the change in the climate variable of interest, calculated as the difference between the future (2070–2099) and historical (1980–2009) period for model  $m$  and scenario  $s$  at longitude  $\lambda$  and latitude  $\phi$ . We consider different response variables, namely, sea level pressure ( $\Delta SLP$ ), zonal winds at 850 hPa ( $\Delta U_{850}$ ),

2-m temperature ( $\Delta T2m$ ), and total precipitation ( $\Delta Pr$ ).  $\Delta Y(m, s)$  is the change in the stratospheric indices which are standardized relative to the intermodel standard deviation within a given scenario before the regression. In addition to  $\Delta U_{10}$  used in Simpson et al. (2018), we also regress surface variables on changes in the polar vortex centroid latitude ( $\Delta PV_\phi$ ) and longitude ( $\Delta PV_\lambda$ ), calculated as described in Section 2.3. Finally,  $a(\lambda, \phi, s)$  and  $b(\lambda, \phi, s)$  denote the regression coefficients obtained using an ordinary least square regression of  $\Delta X(\lambda, \phi, m, s)$  on  $\Delta Y(m, s)$ , and  $\epsilon(\lambda, \phi, m, s)$  is the residual of the linear fit. Before using Equation 7, we first regress out the global-mean  $\Delta T2m(m, s)$  from  $\Delta X(\lambda, \phi, m, s)$  and  $\Delta Y(m, s)$  across models, such that the correlation between  $\Delta X(\lambda, \phi, m, s)$  or ( $\Delta Y(m, s)$ ) and global-mean  $\Delta T2m(m, s)$  across models is zero. This is done to exclude the influence of model climate sensitivity on the analysis which otherwise would obscure the relationship between  $\Delta T2m(\lambda, \phi, m, s)$  and  $\Delta Y(m, s)$ . Note that the relationship between  $\Delta Pr$  and  $\Delta U_{10}$  is largely insensitive to this procedure.

To quantify the potential influence of the stratospheric changes on the surface climate variables several metrics are assessed. First, we assess the regression coefficients  $b(\lambda, \phi, s)$  calculated using Equation 7, which quantify the relationship between the stratospheric and surface variables. Second, we calculate the fraction of variance of  $\Delta X$  across models explained by the regression on  $\Delta U_{10}$  (equivalent to a Pearson correlation coefficient squared). Third, motivated by Simpson et al. (2018), we calculate the fraction of  $4\sigma$  in  $\Delta X$  (roughly corresponding to 2.5%–97.5% of the intermodel spread) that corresponds to the difference between models projecting  $\pm 1\sigma$  of the standardized  $\Delta U_{10}$ . Note that regression analysis does not give a direction of causality and additional information, for example, from controlled nudging experiments such as those performed in previous studies (e.g., Simpson et al., 2018), are necessary to interpret the regression patterns (see Section 3.4).

### 3. Results

#### 3.1. Zonal Mean Change of the Polar Vortex

The projected changes in wintertime zonal mean zonal wind are shown for CMIP5 and CMIP6 in Figure 1. Results from Abrupt-4xCO<sub>2</sub> (Figure 1a) and SSP245 (Figure 1b) simulations are shown because, on average, they, respectively, simulate the largest and smallest global mean warming among the studied experiments, while SSP585 is shown (Figure 1c) because it has GHG forcing comparable to that in CMIP5 RCP8.5 (Figure 1d), allowing for comparison with previous studies. To facilitate the comparison across CMIP6 experiments, the 40 models that performed Abrupt-4xCO<sub>2</sub>, SSP245, and SSP585 simulations are used to construct the ensemble means (Table S1 in Supporting Information S1).

All experiments show a robust (>90% model agreement) strengthening of the subtropical winds from the upper troposphere to the upper stratosphere. This is understood as a thermal wind response to an increased meridional temperature gradient due to a warming upper tropical troposphere and cooling stratosphere. The ensemble mean zonal wind strengthening reaches a maximum around 30°N and 100 hPa and its magnitude (11.7 m/s in Abrupt-4xCO<sub>2</sub>, 4.7 m/s in SSP245, and 7.8 m/s in both SSP585 and RCP8.5) scales approximately linearly with the scenario-mean global warming levels, which are 5.6°C, 2.3°C, 3.8°C, and 3.4°C in these experiments, respectively. These changes correspond to a wind strengthening at 30°N and 100 hPa of approximately 2 m/s per degree of global warming, although the strengthening varies between 1 m/s and 3 m/s per degree of global warming across individual models suggesting different sensitivity of the subtropical winds to global warming in the models.

All experiments show an ensemble-mean weakening of the zonal winds in the polar latitudes (easterly change), both in the troposphere and the stratosphere, consistent with previous studies (e.g., Manzini et al., 2014). However, the weakening is only consistent across models in the troposphere where it may be related to a weakening of the meridional temperature gradient due to Arctic Amplification (Smith et al., 2022; Woollings, 2008). Note that these are zonal-mean changes; zonally varying changes at the 850-hPa pressure level are reported in Section 3.4. Although the easterly change in the polar stratosphere is not consistent across models, it is worth noting that the ensemble mean weakening is of comparable magnitude in all experiments despite considerably weaker GHG forcing in SSP245. Furthermore, the scaling of wind changes for each model ensemble mean by the corresponding global-mean annual mean model ensemble mean  $\Delta T2m(m, s)$  shows that ~80% of the models simulate a stronger negative wind change per degree of warming in the polar stratosphere (or less positive wind change in mid-latitudes) in SSP245 than in Abrupt-4xCO<sub>2</sub> (see Figure S1 in Supporting Information S1). This

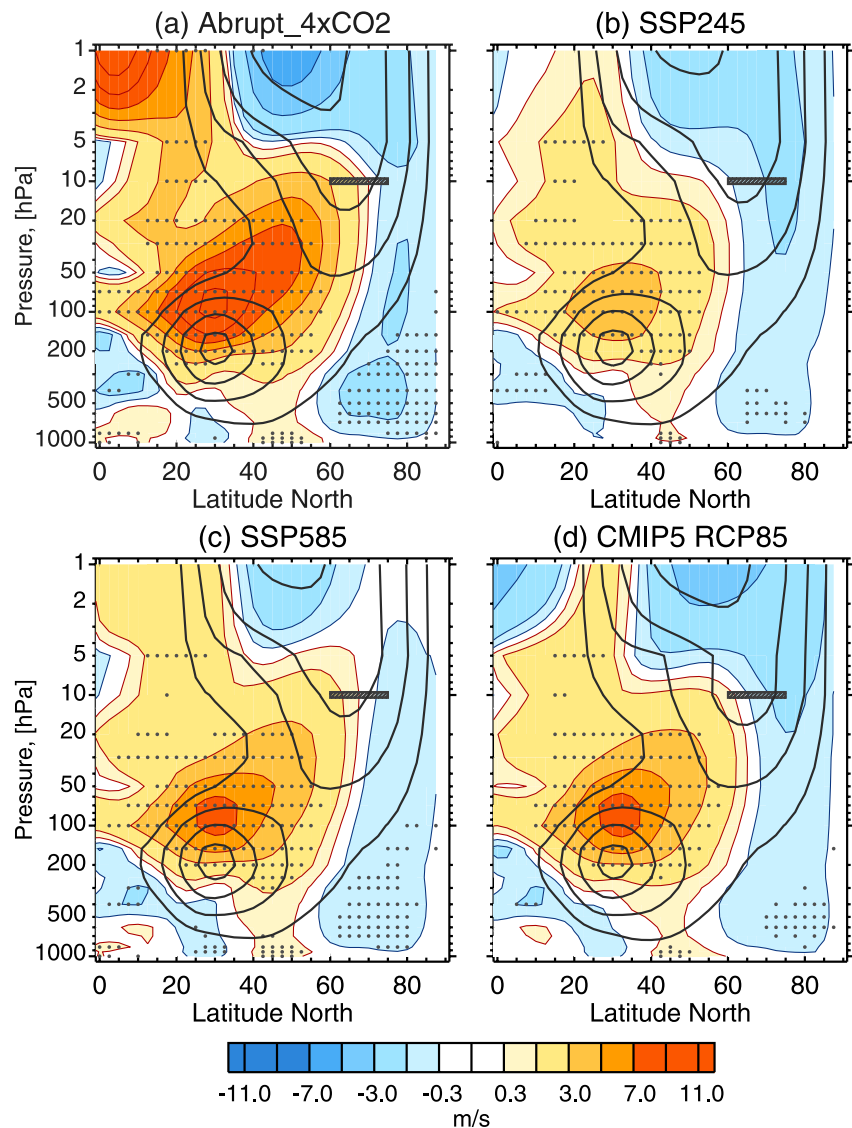


**Figure 1.** Multimodel mean zonal mean zonal wind change for wintertime (December to February, DJF, mean) for (a) Abrupt-4xCO<sub>2</sub>, (b) SSP245 (c) SSP585, and (d) CMIP5 RCP8.5 experiments. Line contours mark ensemble mean climatological winds (10, 20, 30, and 40 m/s). The gray bar at 10 hPa indicates the region used for defining  $\Delta U_{10}$ . Dots indicate areas where at least 90% of the models agree on the sign of the change.

suggests that wind changes are affected by competing factors whose importance varies with global warming levels (Kretschmer et al., 2020; Manzini et al., 2018).

Most previous studies (e.g., Manzini et al., 2014; Simpson et al., 2018) analyzed changes in the stratospheric zonal mean zonal wind in winter. Looking across all seasons (Figure 2), the wintertime (DJF) change has the largest uncertainty by far; however, the uncertainty with respect to sign is present in all seasons. The intermodel spread is smallest in summer when models largely agree on the westerly change of the stratospheric winds. In all seasons, the intermodel spread generally increases with the strength of the forcing. For example, in DJF the spread in SSP585 as defined by the standard deviation is about 50% larger than that in SSP245 (4.3 m/s vs. 2.8 m/s) while in summer (JJA) it is larger by about 30% (0.9 m/s vs. 0.7 m/s). Interestingly, the intermodel difference in  $\Delta U_{10}$  is larger than the differences across scenarios in all seasons. This point will be considered in more detail in the next section. While the difference between the ensemble mean responses across scenarios is insignificant, it is worth noting that, in terms of the median value, the  $\Delta U_{10}$  distribution in CMIP5 RCP8.5 is more comparable to that in the scenarios with weaker forcing (e.g., SSP370 in DJF) than to that in SSP585. This result suggests that model selection may be a more important factor affecting  $\Delta U_{10}$  than the forcing strength.

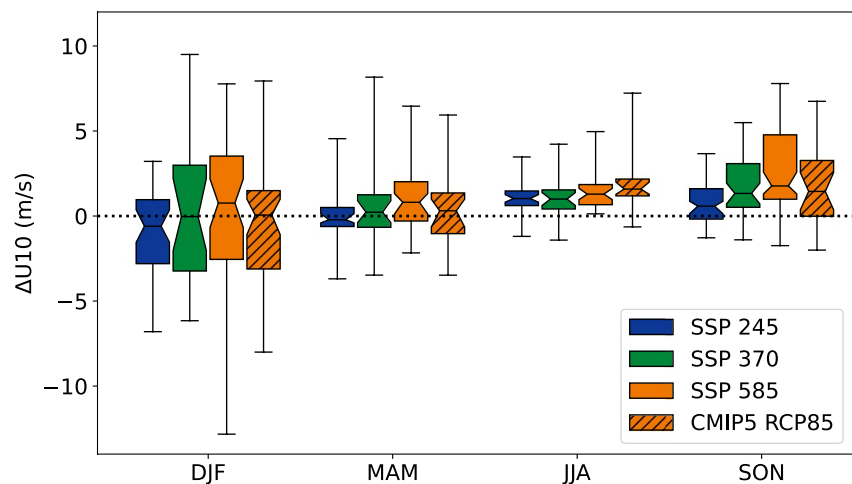


**Figure 2.** Seasonal dependence of the intermodel spread in  $\Delta U_{10}$  in Shared Socioeconomic Pathways (SSP) and CMIP5 RCP8.5 scenarios. The whiskers span the full range of the model ensemble-mean  $\Delta U_{10}$ ; the box extends from the first quartile to the third quartile. The notch indicates the median value of the ensemble means, and the shape/extent of the notch is the confidence interval about the median, which is determined by bootstrapping 5,000 times to determine the 95% confidence interval.

The lack of dependence of  $\Delta U_{10}$  on scenario in DJF is consistent with a weak relationship between  $\Delta U_{10}(m, s)$  and global-mean annual mean  $\Delta T2m(m, s)$  across models in any scenario. A similar result was also noted by Simpson et al. (2018) for CMIP5 RCP8.5. On the other hand we find significant correlations between  $\Delta U_{10}(m, s)$  and global-mean annual mean  $\Delta T2m(m, s)$  across models in JJA ( $r \sim 0.6$ ) and SON ( $r \sim 0.4$ ) in all scenarios, which is consistent with the tendency for the ensemble mean  $\Delta U_{10}$  to increase between SSP245 and SSP585 in these scenarios. In these seasons, the stratospheric winds are less affected by wave driving and more affected by thermodynamic and radiative influences which may be more directly connected to the global warming level. This result may have implications for understanding mechanisms of stratospheric circulation changes; however, it will not be pursued further in this paper. In the rest of the paper, we will focus on the wintertime vortex response where the intermodel spread is the largest and where the downward stratospheric influence on tropospheric circulation is well documented (e.g., Kidston et al., 2015).

Considering DJF, the results shown in Figures 1 and 2 might be interpreted as an indication of low signal to noise ratio in the polar vortex response suggesting that stronger signal and more ensemble members are needed to detect the response. However, individual models do show a significant response and the uncertainty arises largely because individual models do not agree on the sign of the  $\Delta U_{10}$  response. Figure 3 shows  $\Delta U_{10}$  in DJF for individual models and for all analyzed scenarios. The statistical significance of the responses is tested against the null hypothesis of no change using the preindustrial control run for each model following the bootstrapping procedure described in Simpson et al. (2018). Namely, two sets of 30-year chunks, with each set having the same number of chunks as the number of experiment realizations by the model, are randomly sampled from the corresponding preindustrial runs to mimic the past and the future, and the difference between these sets is calculated to mimic the change. The procedure is then repeated 5,000 times to create a distribution of zonal mean zonal wind changes that could occur through sampling of internal variability with a given ensemble size. A model's response is considered to be significant if it lies outside of the 95% confidence interval of this distribution. An assumption here is that the internal variability is not changing dramatically such that the preindustrial control variability is representative of both the future and past periods.

The fraction of CMIP6 models projecting a statistically significant  $\Delta U_{10}$  (whether positive or negative) increases with global warming levels, peaking at 83% in Abrupt-4xCO<sub>2</sub> (Figure 3a), and these models are roughly equally divided between both weakening and strengthening of the vortex in all scenarios except in SSP245 (Figure 3d) where the number of models projecting vortex weakening (30%) is evidently larger than those with vortex strengthening (9%), consistent with a more pronounced weakening seen in the multimodel ensemble mean (Figure S1 in Supporting Information S1). The fraction of models simulating a significant strengthening has increased from 19% in CMIP5 RCP8.5–33% in CMIP6 SSP585. While there are more CMIP6 models with

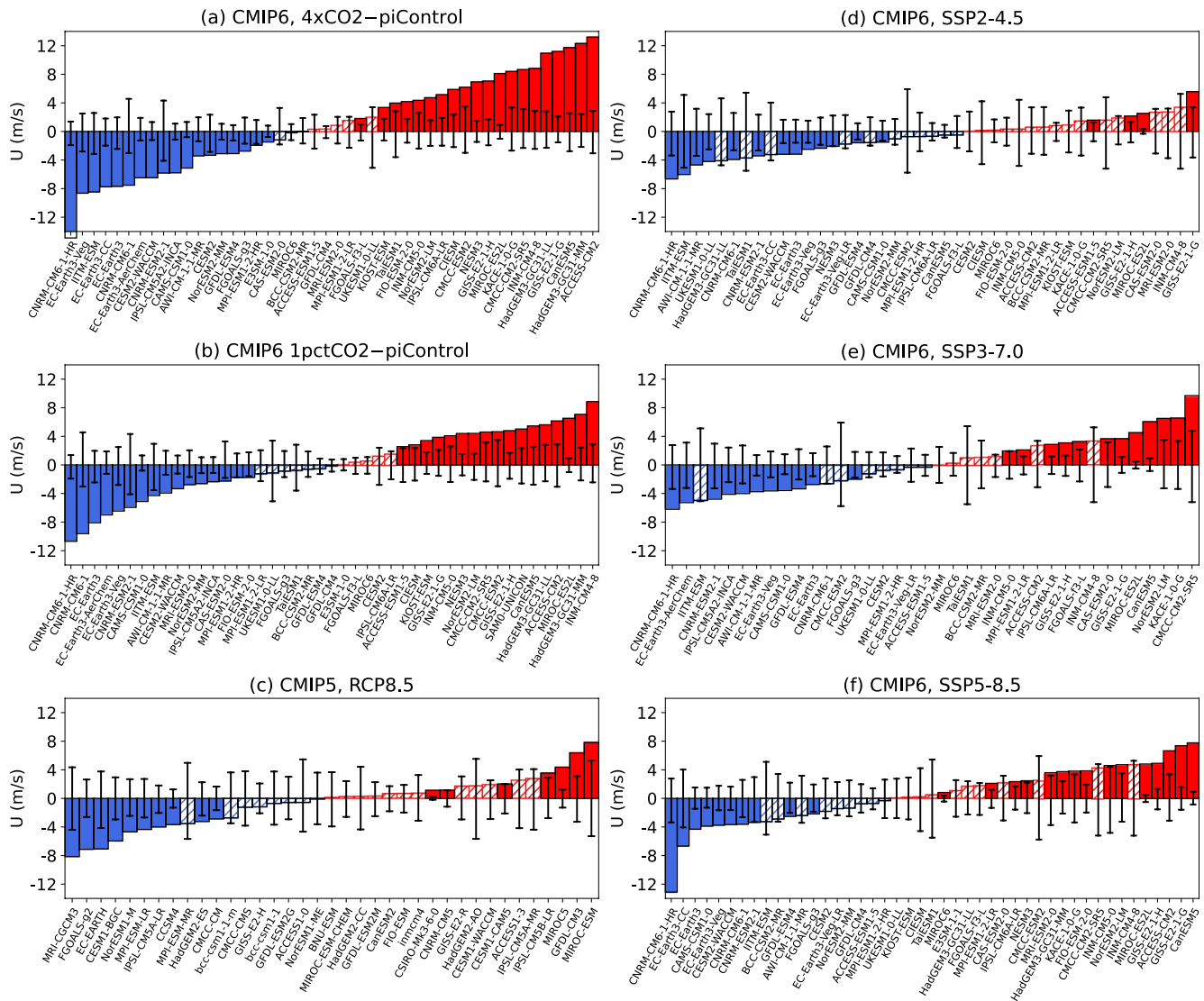


**Figure 3.** DJF  $U_{10}$  changes in individual models and six experiments analyzed in the study. The changes are calculated between (a and b) all years in piControl and years 101–150 of (a) Abrupt-4 $\times$ CO $_2$  and (b) 1%CO $_2$ , and (c–f) 1980–2009 in historical experiments and 2070–2099 in (c) CMIP5 RCP8.5, (d) SSP245, (e) SSP370, and (f) SSP585. The error bars show the 95% confidence interval for  $\Delta U_{10}$ , which is obtained from an equivalent sampling of the piControl and solid/hatched bars indicate models whose  $\Delta U_{10}$  is/is not significant, respectively, according to the method described in the text.

multiple realizations and, consequently, larger signal to noise ratio, this is not the main reason for the increase in the number of models with  $\Delta U_{10}$  exceeding internal variability. Rather, there are more CMIP6 models with a strong positive response. For example, there are seven CMIP6 SSP585 models (16% of all models) having  $\Delta U_{10}$  larger than +4 m/s but only three such models (8% of all models) in CMIP5. At the same time the fraction of models with significant negative  $\Delta U_{10}$  has not changed much from CMIP5 to CMIP6. Among CMIP6 models, CanESM5, GISS-E2-1-G, INM-CM4.8, and ACCESS-CM2 have strongly positive  $\Delta U_{10}$  while CNRM-CM6-1-HR, ITM-ESM, EC-Earth3-CC, and EC-Earth3 have a strongly negative  $\Delta U_{10}$  response in most scenarios. The similarity of model responses across scenarios as well as the partitioning of the response uncertainty into different sources will be discussed in the next session.

### 3.2. Uncertainty Partitioning of the Zonally Averaged Polar Vortex Response

The  $U_{10}$  change in a single realization depends on sampling uncertainty, the particular model response, as well as on the strength of the forcing. Our results indicate that model properties are an important controlling factor as

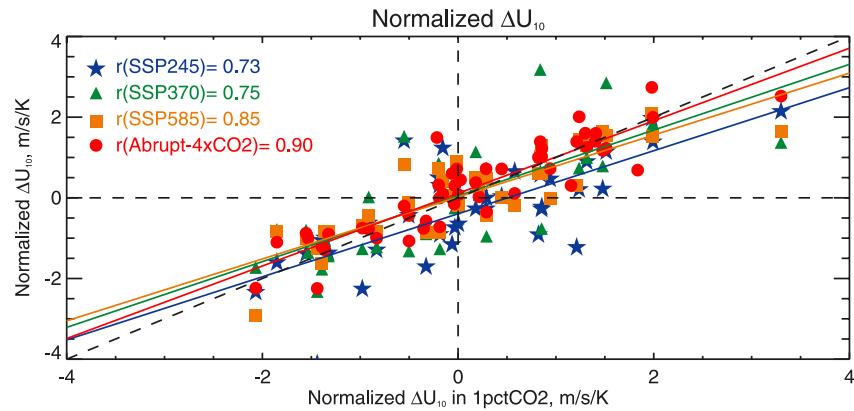


**Figure 4.** Scatterplots of normalized DJF  $\Delta U_{10}$  in individual models and several scenarios as a function of DJF  $\Delta U_{10}$  in the same models in the 1pctCO<sub>2</sub> experiment.  $\Delta U_{10}$  is normalized by the annual mean global warming between the same periods (see Section 2.1 for the information about the periods). The slanted colored solid lines indicate the least-squared linear fits and the slanted dashed line indicates the identity line.

statistically significant responses of both signs are obtained by different models under the same climate forcing. This point is further demonstrated in Figure 4 which shows  $\Delta U_{10}$  in different experiments as a function of  $\Delta U_{10}$  simulated by the same models in the 1pctCO<sub>2</sub> experiment. For comparability between scenarios,  $\Delta U_{10}$  for each

model ensemble mean and for each scenario ( $\Delta U_{10}(m, s)$ ) is normalized by the corresponding global-mean annual mean model ensemble mean  $\Delta T_{2m}(m, s)$ . The responses in different experiments are strongly correlated with correlation coefficients ranging from 0.73 to 0.90. Most models simulate changes of the same sign in all experiments, supporting the hypothesis that model properties strongly affect both the sign and the magnitude of  $\Delta U_{10}$ .

We now quantify the relative contribution of all sources of uncertainty to the projected evolution of the polar vortex. Figure 5 shows the total uncertainty in  $\Delta U_{10}$  and individual uncertainty components calculated following Equations 1–5 (Section 2.2).  $\Delta U_{10}$  is smoothed using a 30-year moving average. At the mid-21st century, internal variability contributes around 80% to the total variance (Figure 5b), with the next largest source of uncertainty from the model response uncertainty that is independent of scenario ( $M$ ). During the second half of the 21st century the total uncertainty increases (Figure 5a), mostly due to the model uncertainty  $M$ . The model uncertainty increases considerably after 2080 and becomes the largest contributor to the total uncertainty by the end of the century. For the end of the century period 2070–2099,  $M$  explains more than 50% of the total variance (Figure 5b). Following Yip et al. (2011) the uncertainty due to the differential response of the models to different scenarios ( $D$ ) is considered separately. Considering  $M$  and  $D$  together, following Hawkins and Sutton (2009), shows that the combined contribution of the model uncertainty exceeds 60%.

Partitioning of the uncertainty in the stratospheric vortex response is in contrast with that of the surface temperature response where, by the end of the century, the scenario uncertainty can be the largest contributor even on regional scales (Hawkins & Sutton, 2009). For the  $U_{10}$  response, the scenario uncertainty does not exceed 10%. One needs to remember that the scenarios considered by Hawkins and Sutton (2009) encompassed a slightly larger range of global warming levels (1.8–3.4 K compared with 2.4–3.8 K here); however, the uncertainty in the sign of the  $U_{10}$  response suggests that the result would not qualitatively change if a similar range of the global warming levels was considered here.

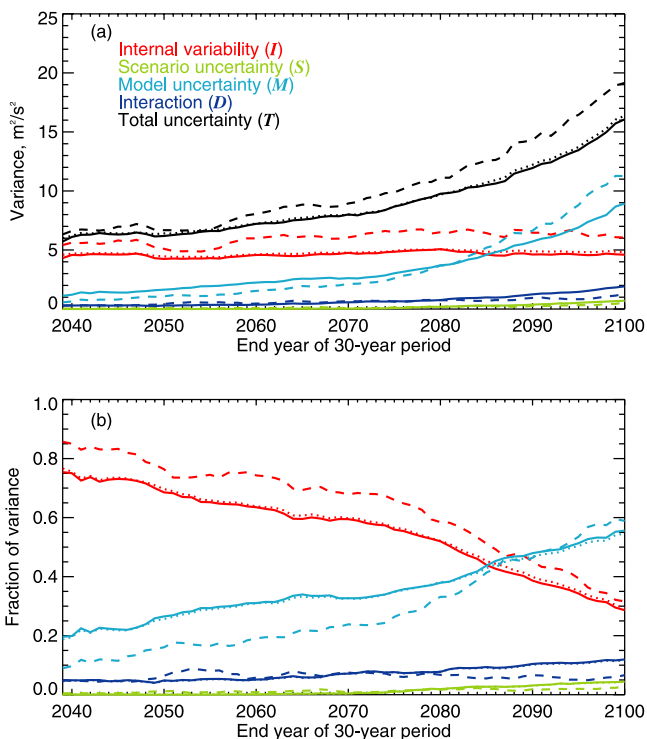


**Figure 5.** Uncertainty partitioning of the 30-year mean  $U_{10}$  changes with respect to the reference period 1980–2009. (a): Absolute values ( $m^2/s^2$ ) of the different sources of uncertainty in the combined  $U_{10}$  wind changes in SSP245, SSP370, and SSP585 scenarios and (b): Relative contribution of different sources of uncertainty to the total variance. Solid lines show variances calculated using all available realizations. Dotted lines show results where internal variability  $I$  is calculated based on Equation 8. Dashed lines show results based on the 11 models having 5 or more realizations in each of the three scenarios (Table S1 in Supporting Information S1).

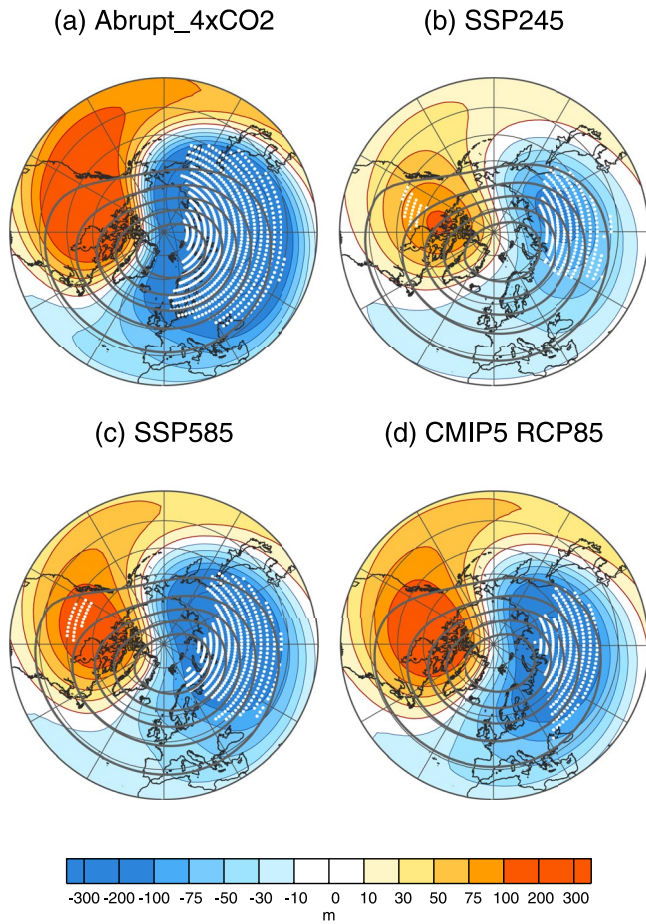


**Figure 6.** Multamodel ensemble mean response of 10-hPa geopotential height ( $\Delta Z_{10}$ ) calculated as the difference between (a) years 100–150 of Abrupt-4xCO<sub>2</sub> and all years of piControl; (b) years 2070–2099 of SSP-245 and 1980–2009 of historical; (c) same as (b) but for SSP-585; and (d) same as (b) but for CMIP5 RCP8.5. Dots indicate areas where 90% of the models agree on the sign of the response. The 40 CMIP6 models with simulations in all three experiments are used in (a–c).

Assessing the contribution of the internal variability is complicated by most models providing only a few realizations, therefore, Equation 1 can lead to a biased estimation of the internal variability (Lehner et al., 2020). To test the sensitivity of the results to the uncertainty in estimating the internal variability, we repeated the calculations in two different ways. First, for the models having fewer than 5 realizations, we estimated the internal variability using their piControl simulations. Here, the internal variability is estimated as the variance of the 30-year mean  $U_{10}$  from the piControl ( $U_{10pi}$ ) multiplied by 2. The multiplication accounts for the fact that the variance of the difference is the sum of the variances of the two terms. Specifically,

$$I(t) = \frac{1}{N_s \cdot N_m} \cdot \sum_{s=1}^{N_s} \sum_{m=1}^{N_m} J(s, m, t) \quad (8)$$

where

$$J(s, m, t) = \begin{cases} \frac{1}{N_r(s, m) - 1} \sum_{r=1}^{N_r(s, m)} [u(s, m, r, t) - \bar{u}(s, m, :, t)]^2 & \text{if } N_r(s, m) \geq 5 \\ 2 \cdot \text{Var}(U_{10pi}) & \text{if } N_r(s, m) < 5 \end{cases}$$

Following this estimation of the internal variability, the total uncertainty  $T$  was calculated not from Equation 5 but as the sum of the four terms (Equation 6) with  $I$  estimated from Equation 8. Applying this approach did not affect the results obtained using the baseline approach (Figure 5).

In the third approach, we repeated the calculations using Equations 1–5 but only used the 12 models with 5 or more realizations in each of the three scenarios (Table S1 in Supporting Information S1). Models with multiple realizations contribute disproportionately strongly to the variances calculated using Equations 1–5. To exclude potential biases due to the varying number of realizations by individual models here we use only the first 5 realizations of each of the 12 models. The total variance, internal variability, and model uncertainty all increase when calculated using this approach (Figure 5). However, the uncertainty partitioning does not change much in comparison to the baseline approach. In summary, the different sensitivity tests led to essentially the same result as the baseline approach, confirming that the model uncertainty is the largest contributor to the total uncertainty by the end of the 21st century.

### 3.3. Zonal Asymmetric Change of the Polar Vortex

Matsumura et al. (2021) demonstrated that CMIP5 models project a robust zonally asymmetrical response in the stratosphere with pronounced cooling over Eurasia and suppressed cooling, or even a warming, over North America. A zonally asymmetric stratospheric response is also robustly detected in the CMIP6 experiments, as seen from  $\Delta Z_{10}$  (Figure 6).

The spatial structure of  $\Delta Z_{10}$  with an anomalous low over Eurasia and anomalous high over North America is remarkably similar across the experiments, although the magnitude varies considerably: the Abrupt-4xCO<sub>2</sub> experiment shows the strongest and SSP245 shows the weakest response. This response is nearly orthogonal in space to the NAM response found in the pioneering work by Shindell et al. (1999), which has since been the focus of most subsequent studies of stratospheric climate change. In all experiments, the response appears less robust in the western hemisphere, in particular, over North America, where models disagree on the positive  $\Delta Z_{10}$ . The disagreement on the sign of the response in the western hemisphere is a consequence of the global stratospheric cooling which causes a shrinkage of the stratosphere (i.e., negative  $\Delta Z_{10}$ ; Pisoft et al., 2021). This offsets the rise in  $Z_{10}$  in the western hemisphere and compounds the fall in  $Z_{10}$  geopotential height in the eastern hemisphere.

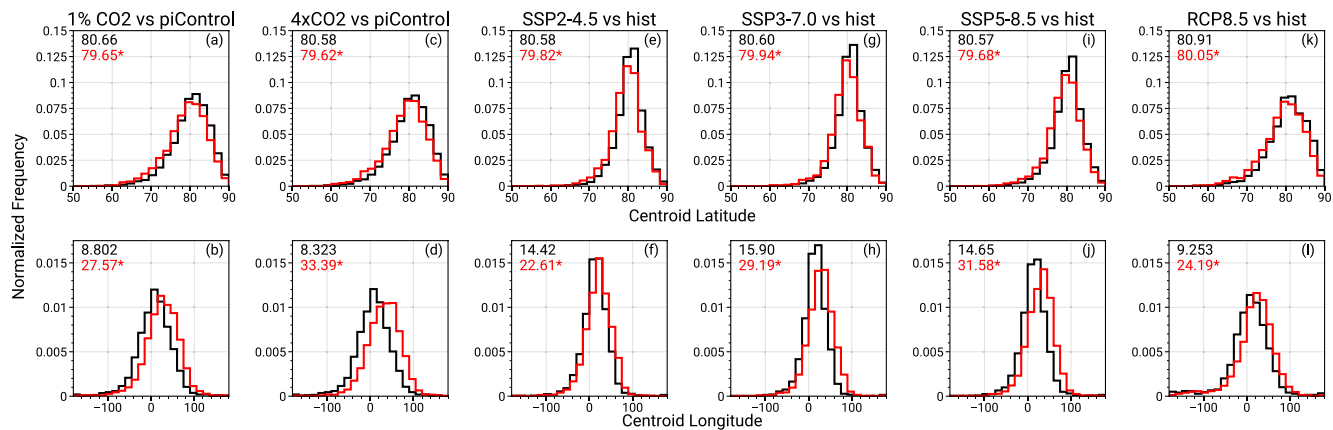


**Figure 7.** Distributions of the DJF polar vortex centroid latitude (top row) and centroid longitude (bottom row) at 10-hPa comparing reference (black) and global warming (red) experiments from CMIP6 (a–j) and CMIP5 (k–l). The medians of each of the distributions are listed in the top left of each panel. In all cases, the distributions are constructed using the centroid values from individual months between December and February. For the 1pctCO2 and Abrupt-4xCO2 experiments (a–d), the distributions are constructed by using only the last 50 years of the preindustrial control (black) or experiment (red) simulations. For the Shared Socioeconomic Pathways (SSP) and RCP experiments (e–l), the distributions for the historical (black) are constructed using only years from 1980 to 2009, while the future scenarios (red) are constructed using only years from 2070 to 2099. The statistical significance of the difference in the medians between the reference and global warming experiments is assessed with a bootstrap test comparing the 95% confidence intervals on the medians. Asterisks on the red numbers indicate that the medians are significantly different.

The magnitude of the stratospheric cooling, as well as the magnitude of the rise in  $Z_{10}$  in the western hemisphere, differ across the models, which leads to the disagreement in the sign of response. Removal of the global mean  $\Delta Z_{10}$  in individual models before constructing the ensemble mean reveals a robust positive change over North America (Figure S2 in Supporting Information S1). Note that, following the approach of Figure 1, only 40 CMIP6 models with simulations in all three experiments are used in Figure 6; however, inclusion of all models does not change the result.

Matsumura et al. (2021) does not give a definitive answer to whether the vortex shift, deduced by Figure 6, occurs mostly along latitude or longitude. To address this question, we analyze changes in the center of the vortex using the moment diagnostics (Section 2.3).

Figure 7 (upper panels) shows the distribution of monthly polar vortex centroid latitudes ( $PV_{\phi}$ ) during winter months. In the preindustrial and historical experiments,  $PV_{\phi}$  is typically located north of  $70^{\circ}\text{N}$  with a median at  $\sim 80^{\circ}\text{N}$ . In all scenario experiments, the median values of the distributions are shifted southward by  $\sim 1^{\circ}$  with only a small difference in the magnitude of the shift between the scenarios. A southward shift of a larger magnitude ( $2.5^{\circ}$ ) was earlier reported for a single CMIP5 model under the RCP8.5 scenario (Mitchell et al., 2012) which is within the intermodel spread in  $\Delta PV_{\phi}$  as found here (see Figure 8).

Similarly, Figure 7 (lower panels) shows the distribution of monthly polar vortex centroid longitudes ( $PV_{\lambda}$ ). In the preindustrial and historical experiments, the vortex center is shifted off the pole toward Europe although the monthly  $PV_{\lambda}$  values span the wide range of longitudes between  $60^{\circ}\text{W}$  and  $80^{\circ}\text{E}$ . A shift of the polar vortex off the pole toward Eurasia is a known feature of the observed stratosphere (e.g., Karpetchko et al., 2005). One can see that an eastward shift in  $PV_{\lambda}$  is simulated in all scenarios. The magnitude of the eastward shift increases with the strength of the forcing ranging between  $\sim 8^{\circ}$  in the median value in the scenario with the weakest forcing (SSP245) and  $\sim 25^{\circ}$  in the scenario with the strongest forcing (Abrupt-4xCO2) where the magnitude of the shift is considerable when compared to the unforced variability in the preindustrial experiment. The shift accelerates slightly with the strength of the warming: the rate of the shift is on average about  $4.5^{\circ}$  per degree of warming in Abrupt-4xCO2 and only  $3.4^{\circ}$  per degree of warming in SSP245; however, the difference in the rate of the shift between the scenarios is not statistically significant. One can also see a more eastward location of the vortex center in the CMIP6 historical ( $14^{\circ}$ – $15^{\circ}\text{E}$ ) than in the CMIP6 preindustrial ( $8^{\circ}\text{E}$ ) or CMIP5 historical ( $9^{\circ}\text{E}$ ) experiments. While the former difference may result from the climate change between preindustrial and historical experiments, the latter difference is due to different model biases between CMIP5 and CMIP6 models. For an overview of the stratospheric biases in the historical simulations of CMIP5 and CMIP6 (see for example, Rao et al. (2022)).

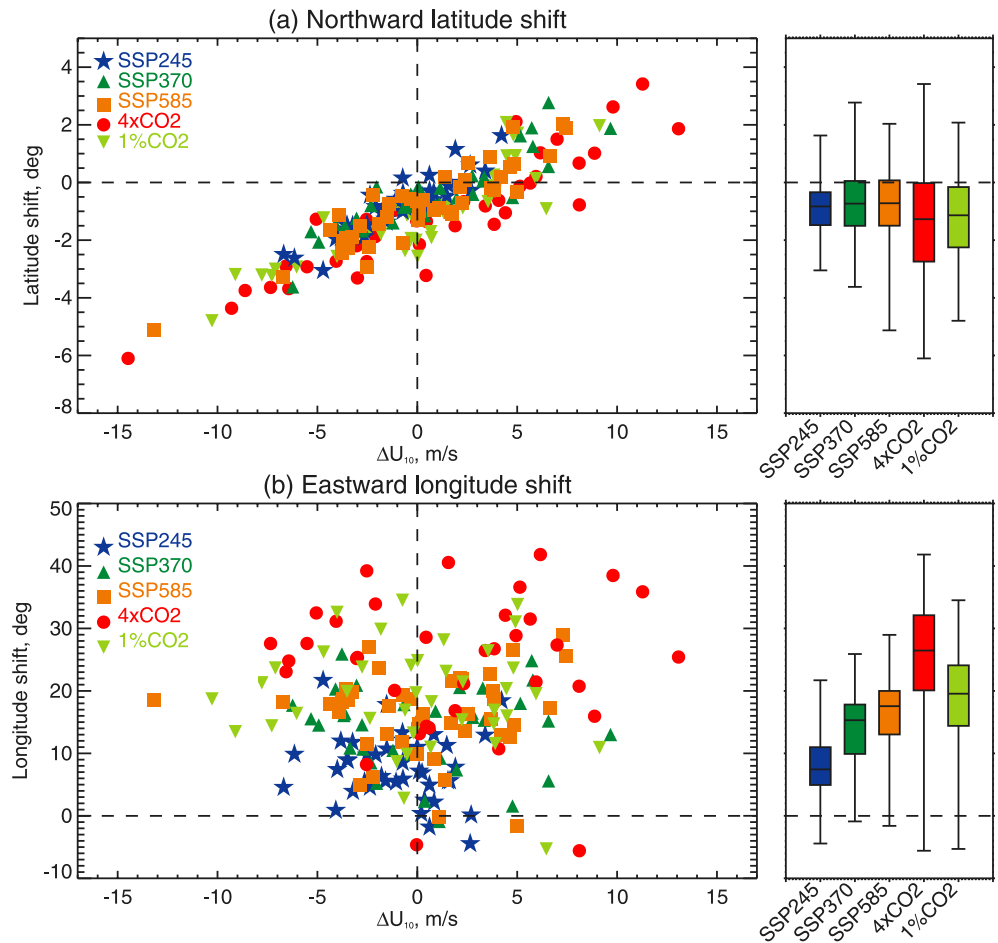


**Figure 8.** Scatterplots and boxplots of the model ensemble-mean changes in DJF polar vortex (a) centroid latitude ( $\Delta PV_{\phi}$ ) and (b) centroid longitude ( $\Delta PV_{\lambda}$ ) against corresponding  $\Delta U_{10}$ . The whiskers in the boxplots shown in the right panels span the full range of the model ensemble-mean changes in the centroid values; the box extends from the first quartile to the third quartile and the bars show the medians.

Figure 8 shows  $\Delta PV_{\phi}$  and  $\Delta PV_{\lambda}$  for individual models against corresponding  $\Delta U_{10}$  values. There is a strong ( $r \sim 0.9$ , Table 1) correlation between  $\Delta PV_{\phi}$  and  $\Delta U_{10}$  indicating that a southward/northward shift of the vortex center corresponds to a zonally averaged vortex weakening/strengthening at  $60^{\circ}\text{N}$  (Figure 8a, left). Such a relationship is consistent with observed weakening of the polar vortex during Sudden Stratospheric Warming (SSW) displacement events (Mitchell et al., 2011). While a southward shift is the most likely change across the models (Figure 8a, right), it appears only in  $\sim 75\%$  of models; thus, the uncertainty in the direction of the latitudinal vortex shift is comparable to the uncertainty in the sign of  $\Delta U_{10}$  (Figures 2 and 3).

Figure 8b shows that most CMIP6 models ( $>95\%$ ) simulate an eastward shift of the polar vortex in response to global warming with a few exceptions discussed below. The dependence of the magnitude of the shift on global

warming level is seen when looking at the differences between the scenarios (Figure 8b, right). On the other hand, the relationship between the magnitude of the eastward shift and global warming level across the models is only significant for Abrupt-4xCO<sub>2</sub> ( $r = 0.41$ ,  $p = 0.05$ ) but not for the other scenarios (not shown). Also, there is no relationship between longitudinal shift and the zonal mean wind changes across the models (Table 1).

The eastward shift of the polar vortex is a manifestation of an eastward shift of the planetary wavenumber 1. Figure 9 illustrates this for the Abrupt-4xCO<sub>2</sub> scenario. In this experiment the shift occurs on two timescales (Figure 9a). During the first 5–10 years a fast response occurs when the wavenumber

**Table 1**  
Correlation Between Model Ensemble-Mean Changes in DJF Polar Vortex Centroid Coordinates and  $\Delta U_{10}$

	4xCO <sub>2</sub>	1pctCO <sub>2</sub>	SSP245	SSP370	SSP585
$\Delta PV_{\phi}$	<b>0.91</b>	<b>0.88</b>	<b>0.90</b>	<b>0.90</b>	<b>0.91</b>
$\Delta PV_{\lambda}$	−0.07	−0.10	−0.13	−0.07	0.04

Note. Correlation coefficients highlighted in bold are significant at  $p = 0.05$ .

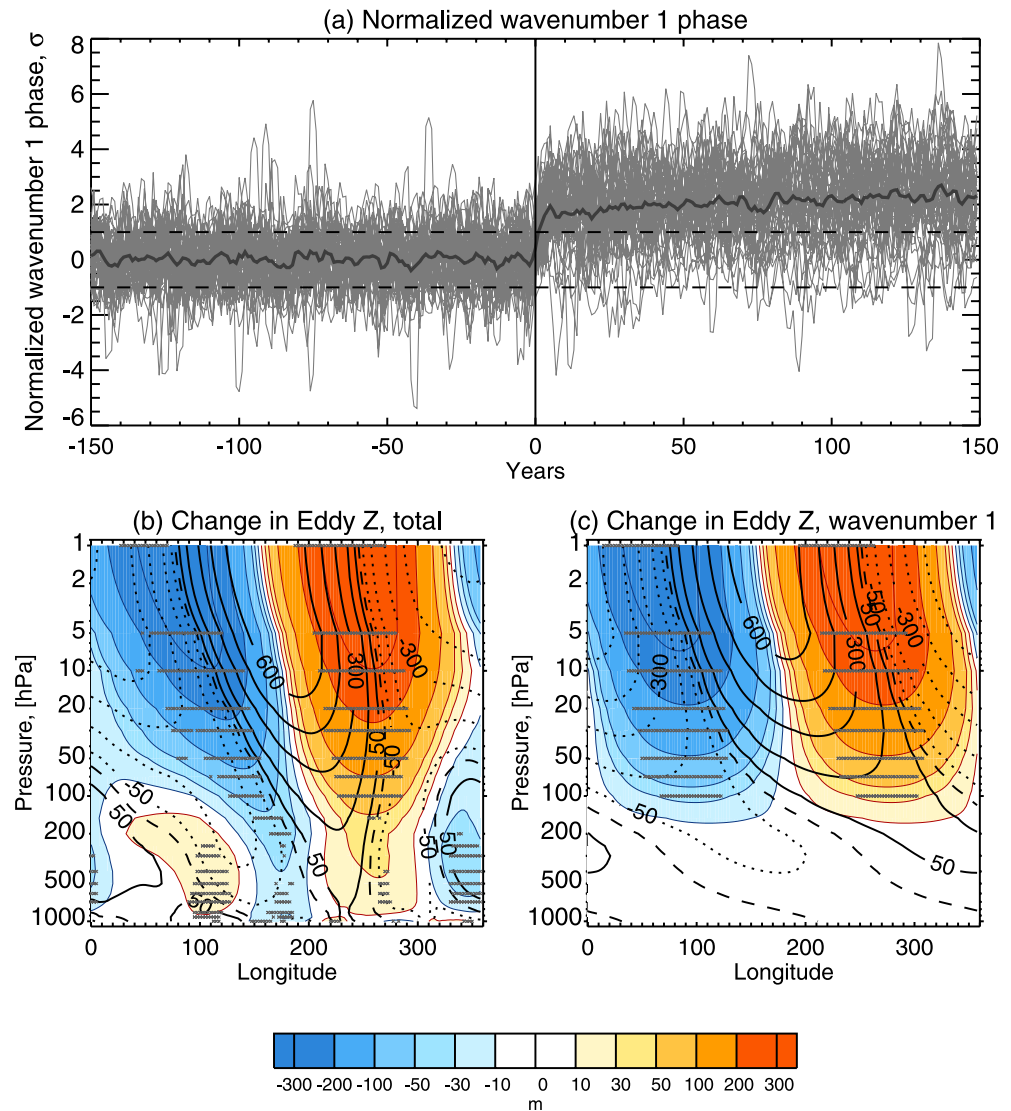


**Figure 9.** (a) Time series of normalized DJF mean wavenumber 1 phases at the 10-hPa geopotential height for all individual models in piControl and Abrupt-4xCO<sub>2</sub> experiments. For each model, the time series are normalized by the standard deviation across all years of the piControl experiment. Thick gray line is the multimodel mean; dashed lines mark  $\pm 1\sigma$ . Year 0 on the  $x$  axis corresponds to the first year of Abrupt-4xCO<sub>2</sub> with negative values corresponding to piControl. (b) Pressure-longitude cross section of DJF eddy geopotential height averaged across 55°–65°N latitudes. Shading shows the difference between years 100–149 of Abrupt-4xCO<sub>2</sub> and all years of piControl. Contours show the piControl climatology in meters with solid/dotted contours showing positive/negative values and dashed line showing zero contour. Gray dots indicate areas where 90% of the models agree on the sign of the response. (c) As in (b) but for wavenumber 1.

1 shifts eastward by a magnitude exceeding, for most models, one standard deviation of its variability in the preindustrial experiment. More than 70% of the shift magnitude reached by years 100–149 of Abrupt-4xCO<sub>2</sub> is reached during the first 5–10 years, that is, during the fast response, while the rest of the response occurs slowly over subsequent decades. The shift is seen as a wavenumber 1 structure tilted westward with height throughout the stratosphere but not in the troposphere where a wavenumber 2 response is seen instead (Figures 9b and 9c). Matsumura et al. (2021) proposed that the zonally asymmetric response in the stratosphere is forced by differential heating in the equatorial Pacific. The wave response shown in Figures 9b and 9c is consistent with the results of their linear barotropic model heating experiments (see Figure 3d in Matsumura et al. (2021)); however, a more detailed investigation of the mechanisms of the shift is needed but beyond the scope of our paper.

While model agreement on an eastward shift is remarkable with more than 95% of models reproducing it when considered across all scenarios (Figure 8b), it is not simulated by all models. BCC-CSM2-MR and MIROC-ES2L

are the two models showing no eastward shift in several scenarios. It is worth noting that these are among the low top models that strongly, by 30%–50%, underestimate the amplitude of the climatological wavenumber 1 in the stratosphere (Table S4 in Supporting Information S1) indicating deficiencies in stratospheric dynamics. Whether these deficiencies contribute to the lack of an eastward shift in the projections is currently not clear, as the mechanism of the shift is not well understood.

### 3.4. Stratosphere-Troposphere Coupling

Stratospheric changes are coupled to those at the surface and uncertainty in projected changes is shown to be linked to regional climate changes (Manzini et al., 2014; Oudar et al., 2020; Scaife et al., 2012; Simpson et al., 2018; Zappa & Shepherd, 2017). Here, we analyze how the coupling with the stratosphere is implicated in the regional climate change uncertainty and explore the differences across the three CMIP6 SSP experiments. Simulations from all models are used for the analysis in this section to improve the robustness of the statistical results. Since not all models performed simulations in all three scenarios, it somewhat affects the interscenario comparison; however, we verified that essentially the same results are obtained if only the models that performed all three SSP experiments are analyzed. Note that the relationships between the tropospheric variables and  $\Delta PV_\varphi$  is very similar to that of  $\Delta U_{10}$  which is expected, given the strong correlation ( $\sim 0.9$ ) between  $\Delta PV_\varphi$  and  $\Delta U_{10}$  (Table 1). The relationships with  $\Delta PV_\varphi$  are reported in Figures S3 and S4 in Supporting Information S1.

We start by looking at the changes in the boreal wintertime (DJF) 850-hPa zonal winds by the end of the 21st century (Figures 10a–10c). In all three scenarios, a tripole structure of the North Atlantic jet changes is detected in the multimodel ensemble mean with strengthening of the jet over Europe and weakening at its northern and southern flanks, although the majority of the models (>90%) agree on the structure of the change only in SSP585 (Figure 10c). The pattern of the multimodel ensemble mean changes is consistent with those found in CMIP3 (Woollings & Blackburn, 2012), CMIP5 (Simpson et al., 2018; Zappa & Shepherd, 2017) and CMIP6 experiments (Harvey et al., 2020; Oudar et al., 2020).

The Pacific jet change is characterized by a poleward shift, also in agreement with previous studies (Barnes & Polvani, 2013; Harvey et al., 2020; Oudar et al., 2020), and the changes at SSP245 and SSP370 are more consistent across models than those of the North Atlantic jet. The ensemble mean  $\Delta U_{850}$  magnitude strengthens with increased emissions indicating that the models show a better agreement in their response to drivers of the jet changes than they do in the response of the stratospheric polar vortex (Section 3.1). In all scenarios,  $\Delta SLP$  consists of a lowering of the Arctic SLP and rising of the mid-latitude SLP (Figure 11), consistent with the poleward shift of the jets, and the magnitude of the response also strengthens with increased emissions.

The middle columns of Figures 10 and 11 show regression coefficients  $b(\lambda, \phi)$  (see Equation 7) used to quantify the relationships between  $\Delta U_{10}$  and  $\Delta U_{850}$  (Figure 10) and  $\Delta SLP$  (Figure 11). Consistent with CMIP5 studies, strengthening of the polar vortex coincides with a poleward shift of the Atlantic and Pacific jet streams and lowering of the Arctic SLP. This is an expected outcome and, although regression does not allow establishing causality, a similar jet shift is simulated in experiments where the stratosphere was nudged to mimic polar vortex responses on opposite ends of the model spectrum (Simpson et al., 2018) where the shift can be unequivocally interpreted as an adjustment of the tropospheric circulation to changes in the stratospheric zonal mean circulation. Interestingly, the relationship with stratospheric changes appears stronger in the North Pacific than in the North Atlantic in both  $\Delta U_{850}$  and  $\Delta SLP$ . While both jets respond qualitatively similarly to an SSW-like stratospheric forcing in stratospheric nudging experiments (Hitchcock & Simpson, 2014), the response in the Pacific jet is expected to be weaker than that in the Atlantic jet, possibly because the northern Pacific precursor of stratospheric changes (Garfinkel et al., 2010) impacts the SSTs in a way that prevents the jet from being affected by the stratospheric anomalies (Dai & Hitchcock, 2021). Thus, if the polar vortex response to climate change is not induced by the Pacific precursors, the Pacific anomalies in Figures 10 and 11 may be interpreted as a response to stratospheric changes. On the other hand, the response of the Aleutian low to climate change has been interpreted as a driver of the polar vortex weakening in AMIP experiments (Karpechko & Manzini, 2017), making a causal interpretation of the relationships in the Pacific difficult.

Figures 10 and 11 (right panels) show the relationship between  $\Delta PV_\lambda$  and  $\Delta U_{850}$  (Figure 10) and  $\Delta SLP$  (Figure 11). In all scenarios the coupling is more pronounced in the eastern hemisphere where the eastward shift of the polar vortex corresponds to a strengthening of the zonal winds over northern Eurasia, a lowering of SLP over the eastern

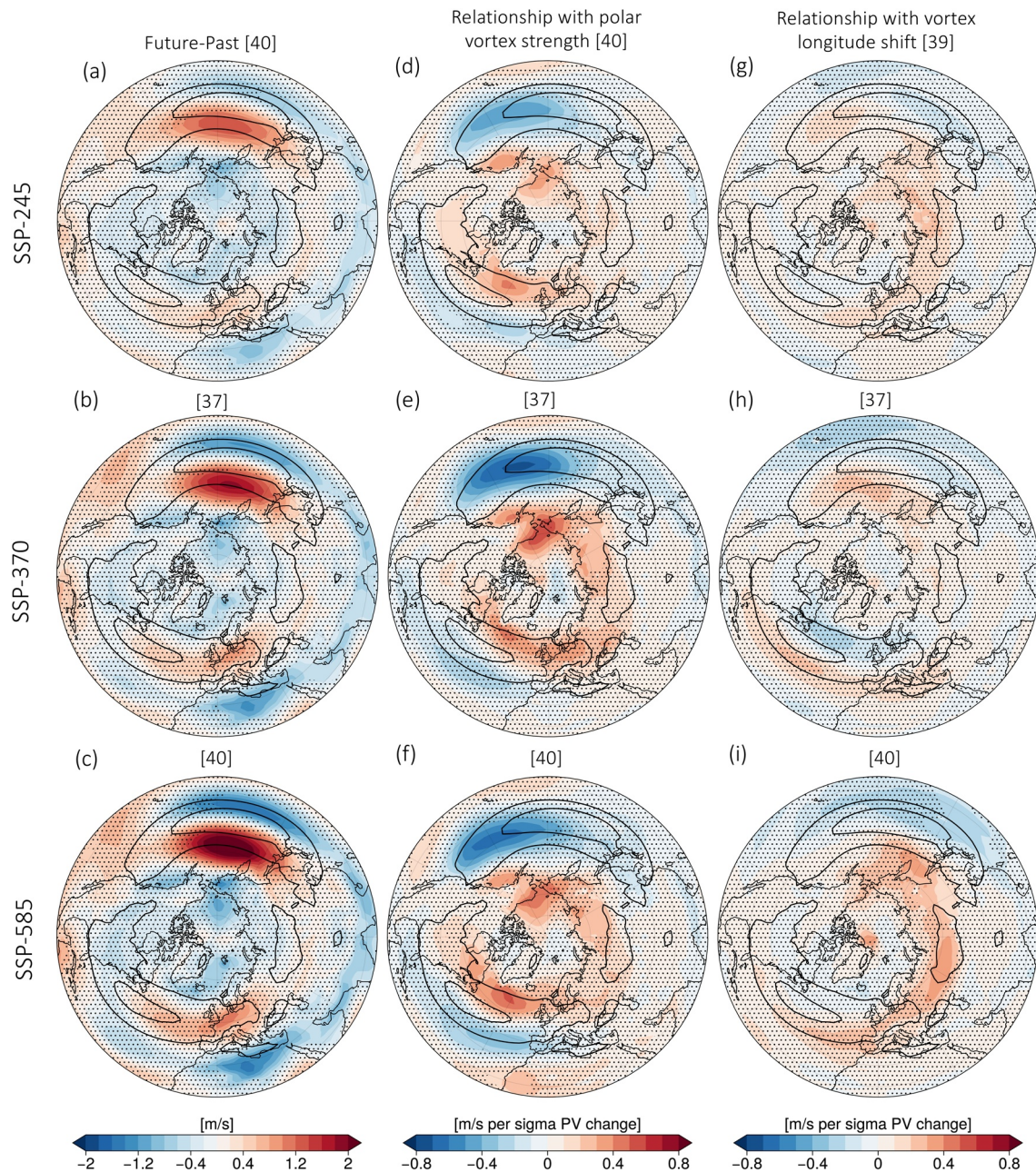


**Figure 10.** (a–c) The  $U_{850}$  changes between 1980–2009 and 2070–2099; (d–i) regression coefficients of  $\Delta U_{850}$  on (d–f)  $\Delta U_{10}$  and (g–i)  $\Delta PV_{\lambda}$  in (a, d, and g) SSP245, (b, e, and h) SSP370, and (c, f, and i) SSP585 after regressing out global warming. Stippling indicates (a–c) areas where less than 90% of the models agree on the sign of the change and (d–i) the regression coefficients are not statistically significant at the 95% confidence level according to a field significance test (Wilks, 2016). The number of models used for the analysis is shown above the panels. Black contours correspond to the climatological mean  $U_{850}$  in the historical simulations (contours from 5 m/s, plotted every 5 m/s).

Arctic and rising of SLP over the northwestern Pacific. The coupling is insignificant in SSP245 and SSP370 but it strengthens and becomes significant in SSP585, consistent with larger  $\Delta PV_{\lambda}$  in this experiment (Figure 8).

Figure 12 is similar to Figure 10 but for projected precipitation ( $\Delta Pr$ ) changes. The precipitation changes (Figures 12a–12c) are consistent with those in CMIP5 and earlier studies (e.g., Simpson et al., 2018; Zappa & Shepherd, 2017): there is drying of the subtropics, in particular over the Mediterranean, and wetting of mid- and polar latitudes. In most regions, for example, Northern Europe or Mediterranean, the changes are driven by changes in the westerly winds and associated moisture fluxes. As is known (e.g., Collins et al., 2013),

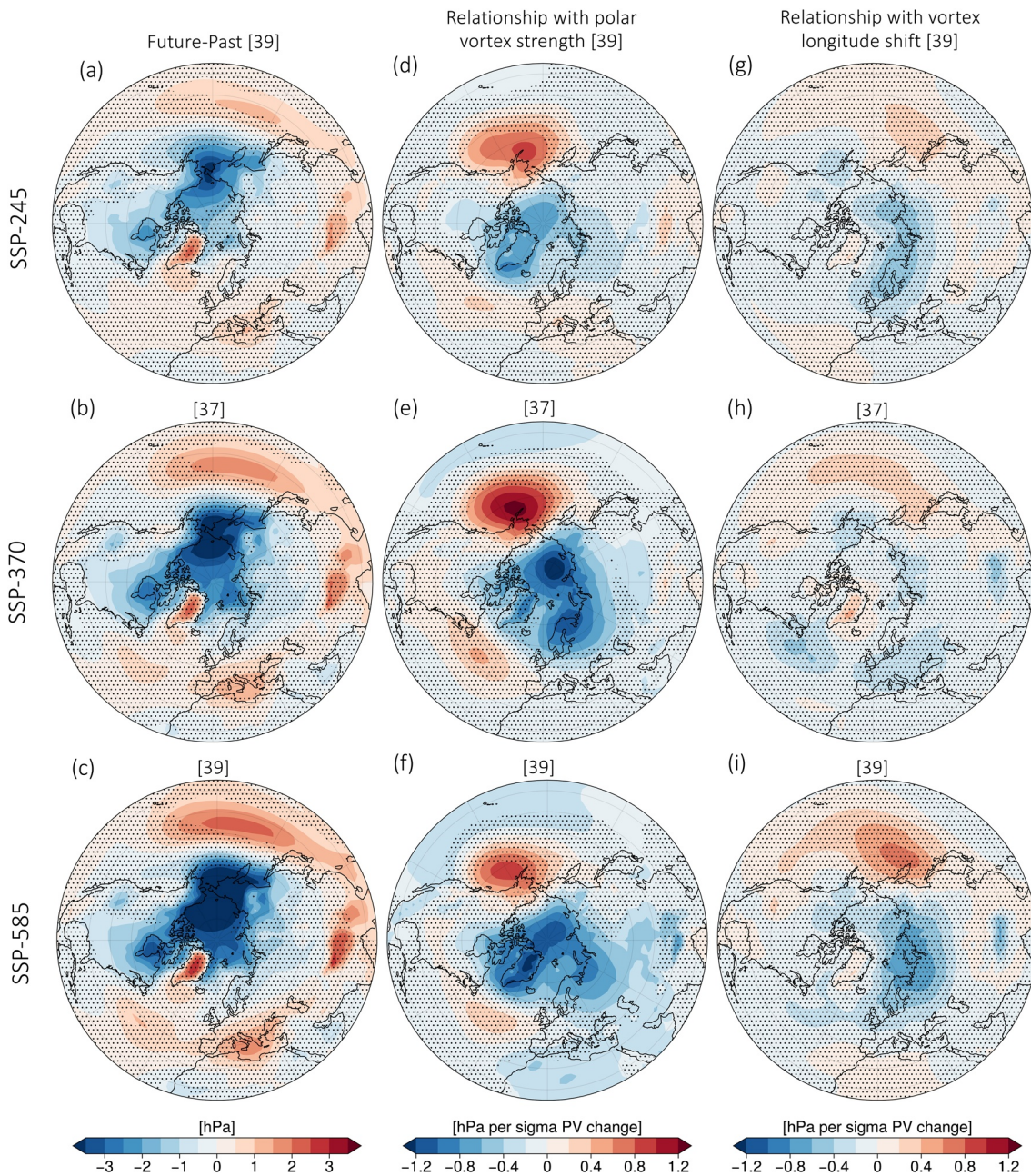


**Figure 11.** Same as Figure 10 but for  $\Delta$ SLP.

precipitation changes amplify with warmer temperatures and higher emission scenarios. The  $\Delta$ Pr relationship to  $\Delta U_{10}$  (Figures 12d–12f) is fairly independent of scenario and maximizes in regions where  $\Delta U_{850}$  is also coupled to  $\Delta U_{10}$ . Note that the  $\Delta$ Pr relationship to  $\Delta U_{10}$  only weakly depend on whether the influence of the global mean  $\Delta T_{2m}$  is removed (Section 2.4). Over the Iberian Peninsula where the multimodel ensemble mean response for all scenarios shows small changes except for drying in the southwestern part,  $\Delta U_{10}$  becomes a key factor affecting the sign of  $\Delta$ Pr with a strengthening/weakening polar vortex consistent with a drying/wetting peninsula (Table 2). In this region, about 10%–20% of the intermodel spread in  $\Delta$ Pr is statistically related to the spread in  $\Delta U_{10}$  with some dependence on scenario (Table 2). These values are somewhat larger than those reported by Simpson et al. (2018), partly because of the differences in the boxes used to define the region (Figure 12).

Similar to  $\Delta U_{850}$  (Figure 10),  $\Delta$ Pr relationship with  $\Delta U_{10}$  is also strongest over the Pacific, a feature that was not given attention in previous studies. While the multimodel ensemble mean  $\Delta$ Pr over the coast of northwestern

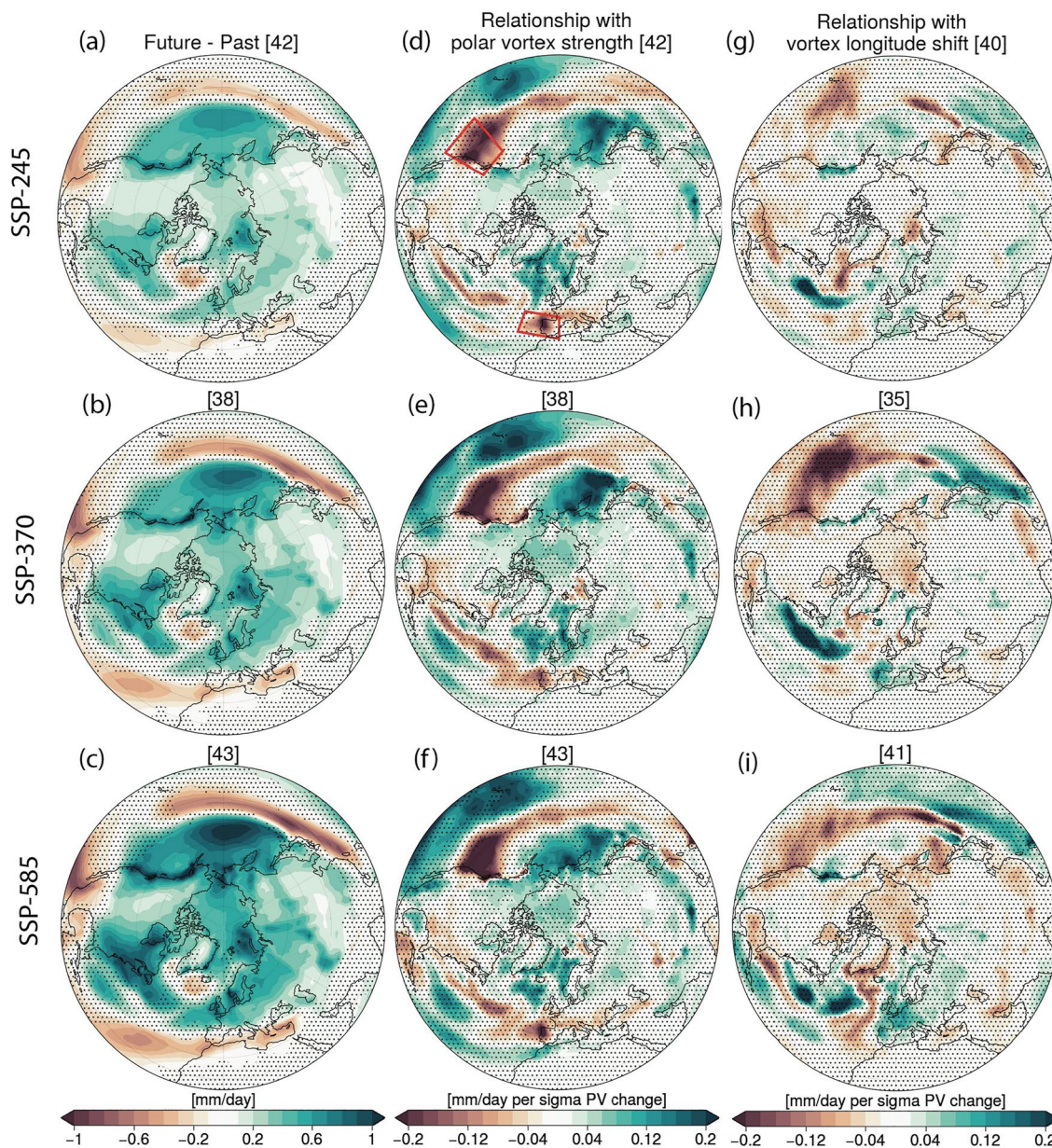


**Figure 12.** Same as Figure 10 but for  $\Delta Pr$ . Red boxes in (d) mark regions referred to in Table 2.

US and British Columbia shows wetting of  $\sim 0.3$  mm/day to  $\sim 0.5$  mm/day for SSP245 and SSP585, respectively, the modulation by  $\Delta U_{10}$  is about  $\pm 30\%$  of the multimodel mean anomaly with models projecting polar vortex strengthening also projecting less wetting than the models with weakening polar vortex (Table 2). There is also a significant relationship of  $\Delta Pr$  to  $\Delta U_{10}$  over the North Pacific. Since precipitation changes can affect ocean circulation (e.g., Levang & Schmitt, 2015), this result reveals a potential new pathway for coupling between stratospheric and ocean circulation changes, in addition to earlier identified influences from stratosphere-induced temperature and wind stress anomalies (e.g., Reichler et al., 2012). The relationship between  $\Delta Pr$  and  $\Delta PV_{\lambda}$  is more pronounced in the western Northern Atlantic and eastern Pacific; however, it is not statistically significant in any scenario (Figure 12).

We next consider the relationship between  $\Delta T2m$  and  $\Delta U_{10}$  (Figure 13). Note that such an analysis study has not previously been done, although the sensitivity of  $\Delta T2m$  to projected NAM changes has been shown (e.g., Karpechko, 2010). The intermodel spread in  $\Delta T2m$  is strongly controlled by global mean warming across models; therefore, the global mean  $\Delta T2m$  has been regressed out before the analysis (Section 2.4).  $\Delta T2m$  is characterized

**Table 2**  
Influence of the Stratospheric Polar Vortex Change on Precipitation ( $\Delta\text{Pr}$ ) and Surface Temperature ( $\Delta T2m$ ) Change

		$\Delta\text{Pr}$	$\Delta\text{Pr}(\Delta U_{10-})$	$\Delta\text{Pr}(\Delta U_{10+})$	$\beta$	$\sigma^2$	$4 \times \sigma$
Iberia	SSP245	<b>0.07</b>	<b>0.07</b>	<b>-0.07</b>	<b>-0.08</b>	20	22
	SSP370	-0.02	<b>0.10</b>	<b>-0.10</b>	<b>-0.08</b>	11	16
	SSP585	0.00	<b>0.13</b>	<b>-0.14</b>	<b>-0.08</b>	13	18
North West US	SSP245	<b>0.31</b>	<b>0.13</b>	<b>-0.13</b>	<b>-0.12</b>	18	21
	SSP370	<b>0.36</b>	0.08	-0.08	<b>-0.12</b>	15	19
	SSP585	<b>0.53</b>	<b>0.17</b>	<b>-0.18</b>	<b>-0.15</b>	18	21
		$\Delta T2m$	$\Delta T2m(\Delta U_{10-})$	$\Delta T2m(\Delta U_{10+})$			
Northern Eurasia	SSP245	<b>4.18</b>	<b>-0.20</b>	<b>0.18</b>	<b>0.29</b>	23	24
	SSP370	<b>5.85</b>	<b>-0.28</b>	<b>0.30</b>	<b>0.34</b>	32	28
	SSP585	<b>7.46</b>	-0.14	0.15	0.19	6	12
Western US	SSP245	<b>3.35</b>	<b>0.24</b>	<b>-0.19</b>	<b>-0.17</b>	9	15
	SSP370	<b>4.28</b>	0.10	-0.11	-0.15	6	12
	SSP585	<b>5.37</b>	<b>0.23</b>	<b>-0.25</b>	<b>-0.36</b>	22	23

*Note.* Values are calculated for  $\Delta\text{Pr}$  over Iberia and adjacent Atlantic ocean ( $35^\circ\text{N}$ – $45^\circ\text{N}$ ,  $340^\circ\text{E}$ – $360^\circ\text{E}$ ) and Northwest US and adjacent Pacific ocean ( $30^\circ\text{N}$ – $50^\circ\text{N}$ ,  $220^\circ\text{E}$ – $240^\circ\text{E}$ ) and for  $\Delta T2m$  over Northern Eurasia ( $40^\circ\text{N}$ – $70^\circ\text{N}$ ,  $80^\circ\text{E}$ – $130^\circ\text{E}$ ) and Western US ( $35^\circ\text{N}$ – $50^\circ\text{N}$ ,  $235^\circ\text{E}$ – $270^\circ\text{E}$ ). Shown are ensemble mean change in  $\Delta\text{Pr}$  [mm/day] and  $\Delta T2m$  [K], anomalous (with respect to the multimodel mean after regressing out global mean temperature change across models) mean change across models with ( $\Delta U_{10-}$ ) weakening or ( $\Delta U_{10+}$ ) strengthening of the polar vortex, regression coefficient ( $\beta$ ) of  $\Delta\text{Pr}$  [mm/day] and  $\Delta T2m$  [K] on  $\Delta U_{10}$ , fraction of the variance ( $\sigma^2$ ) explained by the regression of  $\Delta\text{Pr}$  and  $\Delta T2m$  on  $\Delta U_{10}$  [%], and fraction of the  $4\sigma$  ( $\sim 2.5$ – $97.5\%$ ) intermodel spread ( $4\sigma$ ) that corresponds to the difference between models projecting  $\pm 1\sigma$  of the standardized  $\Delta U_{10}$  [%]. For ensemble mean changes and regression coefficients, bold values indicate values significantly different from 0 ( $p = 0.05$ ). For mean changes corresponding to the models with weakening or strengthening polar vortex, bold values indicate values significantly different from each other. In all cases significance is tested according to a two-sided Student's  $t$ -test at  $p = 0.05$ .

by global surface warming with Arctic amplification, and the magnitude of warming increases with higher emission scenarios. For all scenarios, the  $\Delta T2m$  relation with  $\Delta U_{10}$  is strong over the North Pacific where projected polar vortex strengthening is associated with anomalous warming. Weakened advection of cold Siberian air mass due to anomalous  $\Delta U_{850}$  (Figure 10) is the likely explanation for the  $\Delta T2m$  anomaly there, although other plausible factors such as reduced cloudiness and increased shortwave radiative heating associated with the positive  $\Delta\text{SLP}$  anomaly in this region (Figure 11) may also contribute.

A warming anomaly associated with a greater increase in polar vortex strength is seen in eastern Siberia in SSP245 and SSP370 but is weakened in SSP585. Here, the temperature is known to be impacted by stratosphere-related changes in the NAM. Namely, vortex strengthening/weakening is associated with positive/negative NAM and a relative warming/cooling over Siberia as expected from stratospheric nudging experiments (Hitchcock & Simpson, 2014). Similarly, warming anomalies in parts of the eastern US and Canada and cooling over the central and western US resemble those found in stratospheric nudging experiments (Hitchcock & Simpson, 2014) and are consistent with the response to a positive NAM trend found in CMIP3 models (Karpechko, 2010). Note that the cooling anomaly over the western half of the US has not been given attention in the previous studies. This anomaly is likely associated with an anomalous northerly flow related to the high SLP anomaly over the North Pacific and low SLP anomaly over Northern Canada (Figures 11d–11f).

The regression patterns differ between scenarios, partly reflecting sensitivity to model selections. The difference between models with contrasting  $\Delta U_{10}$  responses reaches 0.5 K, or 10% of the ensemble mean  $\Delta T2m$  response, in eastern Siberia in SSP370 and in the western half of the US in SSP585 (Table 2). The fraction of the intermodel spread in  $\Delta T2m$  that can be statistically related to the spread in  $\Delta U_{10}$  varies between 6% and 32% depending on the scenario and metric used (Table 2). Unlike the ensemble mean  $\Delta T2m$  which gets stronger for larger emissions, there is no clear dependence of the  $\Delta T2m$ – $\Delta U_{10}$  relationship on scenario, suggesting that the relationship is affected by model selection and internal variability.

A strong relationship between  $\Delta T2m$  and  $\Delta U_{10}$  is also seen over the Arctic; however, interpretation of these anomalies is not straightforward because they may be associated with both upward and downward coupling. Over the Barents-Kara Seas, positive  $\Delta U_{10}$  is associated with reduced warming, and by inference, reduced sea

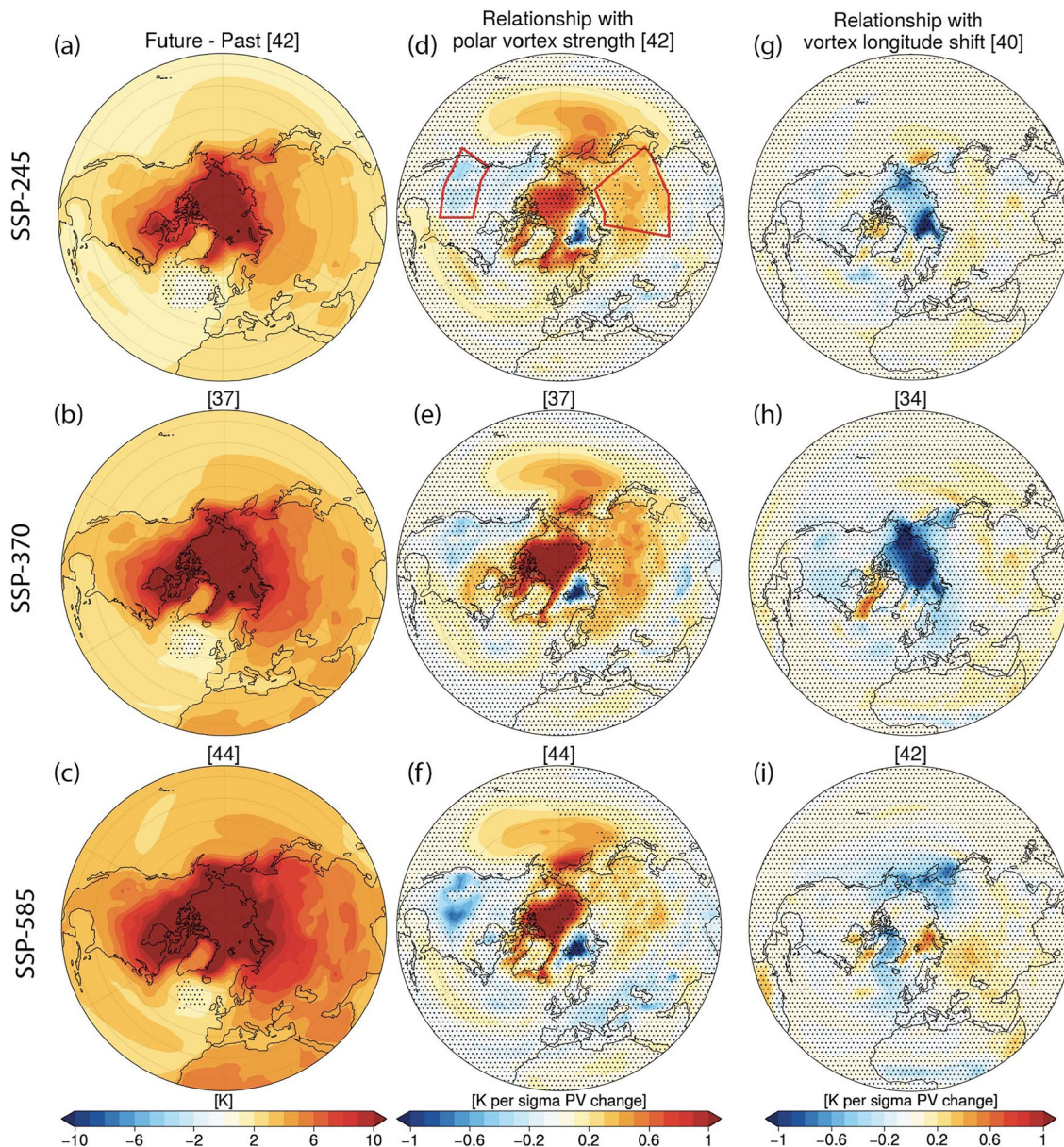


**Figure 13.** Same as Figure 10 but for 2-m temperature. Red boxes in (d) mark regions referred to in Table 2.

ice melting in the region. Since sea ice melting in the Barents-Kara Seas is expected to lead to a vortex weakening (Kretschmer et al., 2020; Manzini et al., 2018; Sun et al., 2015), the negative anomaly is consistent with an upward coupling. The positive anomaly in the central and eastern Arctic is less clear. This anomaly coincides with the negative anomaly in  $\Delta SLP$  (Figure 11) and positive anomaly in  $\Delta Pr$  (Figure 12) and may therefore point to an increased cloudiness and anomalous warming by the longwave radiation. This interpretation relies on the assumption that increased Arctic cloudiness leads to a surface warming; however, the influence of the Arctic clouds on surface temperatures is uncertain (Middlemas et al., 2020).

The eastward polar vortex shift is consistent with a cooling in the eastern Arctic; however, this relationship is not significant in any scenario (Figure 13). Matsumura et al. (2021) proposed that the polar vortex shift will lead to an anomalous cooling over Eurasia. Our results indicate that an anomalous cooling over Eurasia can be associated with a polar vortex weakening (Figure 13) and a southward shift (Figure S4 in Supporting Information S1). However, changes in the polar vortex strength and latitudinal position are less robust across models; therefore, the implication of the projected stratospheric changes for Eurasian surface temperatures is uncertain.

#### 4. Discussion and Conclusions

Earlier studies have established that future projected changes in the wintertime Northern Hemisphere zonal mean stratospheric polar vortex are highly uncertain and that this uncertainty translates into uncertainty in regional climate projections, particularly over Europe. Here, we demonstrate that the uncertainty in polar vortex change projections has not been reduced in CMIP6 experiments. In all experiments, except SSP245, roughly equal number of models project significant weakening and strengthening of the polar vortex. This indicates that the uncertainty in polar vortex strength projections does not arise due to a low signal to noise ratio but is instead strongly contributed by a potentially reducible model uncertainty.

We show that, by the end of the 21st century, approximately half of the spread in the polar vortex projections is due to the model uncertainty, with a smaller role of the irreducible climate noise (internal variability) and a still smaller ( $\sim 10\%$ ) contribution from the scenario uncertainty. While these estimates may be biased due to inaccurate separation between forced and unforced signals in models that provide very few individual realizations (Lehner et al., 2020), calculations using only models with multiple realizations confirm the dominant contribution of the model uncertainty, which was also noticed in CMIP5 models (Manzini et al., 2014). In SSP245, there are more models projecting significant polar vortex weakening than models projecting strengthening. Such an asymmetry, not seen in the other scenarios, may indicate different mechanisms of polar vortex change operating at different global warming levels, for example, Arctic sea ice melting, and consequent nonlinearity in the response as noted in Manzini et al. (2018) and Kretschmer et al. (2020). Note that also non- $\text{CO}_2$  forcing, such as stratospheric ozone recovery, can affect polar vortex changes in SSP245; however, its influence on the Arctic polar vortex is estimated to be weak in comparison to internal variability (Karpechko et al., 2018). Also, anthropogenic aerosol emissions could probably affect the stratospheric wind response because they lead to changes in extra-tropical changes which could alter the planetary wave driving of the stratospheric circulation (Allen & Sherwood, 2010). However, the differences in how the models treat the aerosol-forced response is probably only a secondary factor since the intermodel spread in the stratospheric wind response is also large in simulations with  $\text{CO}_2$  forcing only.

Our results confirm a significant relation between the changes in the zonal mean polar vortex strength and climate over Europe reported in other studies (Manzini et al., 2014; Scaife et al., 2012; Simpson et al., 2018), but also emphasize the coupling in other regions. By the end of the 21st century, the uncertainty in the polar vortex strength projections is related to up to 20% of the intermodel spread in projected precipitation over the Iberian Peninsula and northwestern US. While projected 2-m temperatures strongly depend on model's climate sensitivities, we show that after regressing its influence out, up to 20% of the spread in projected 2-m temperatures over the western half of the US and up to 30% over Northern Eurasia can be associated with the uncertainty in the projected polar vortex strength. Simpson et al. (2018) used nudging experiments to confirm that the regression patterns of precipitation over Europe are consistent with downward influence of the polar vortex strength changes, and a similar analysis needs to be done for the other regions to attribute the causes of the relationship.

Although the zonal mean polar vortex response is highly uncertain, we find a remarkable consistency across models in simulating an eastward shift of the polar vortex, which is interpreted as an eastward shift of the climatological wavenumber 1. Our results are consistent with those by Matsumura et al. (2021) who showed an asymmetry in the stratospheric response in CMIP5 models. We further show that the shift appears in all studied emission scenarios and its magnitude generally increases with global warming level, although only a small fraction of the intermodel spread can be attributed to the model's climate sensitivity. A few models, however, do not project the eastward shift. We suggest that the divergent stratospheric projections by these models might be related to deficiencies in their simulated stratospheric variability, such as strongly underestimated amplitude of the stratospheric wavenumber one in historical simulations; however, we emphasize that obtaining conclusive results would require a more detailed investigation which goes beyond the scope of the present paper.

Climate models also project a small southward shift of the polar vortex of about  $1^\circ$  in the multimodel ensemble mean in all scenarios; however, unlike the eastward shift, the southward shift is projected by only  $\sim 75\%$  of the models, that is, it is less robust. The magnitude and direction of the latitudinal shift strongly correlate with the change in the zonal mean stratospheric wind strength across models ( $r \sim 0.9$ ) suggesting that these two indices reflect essentially the same process. The correlation between the indices, and, consequently, their similar relationship with the surface changes, raises the question which of the two factors—changes in the zonal mean winds or the latitudinal shift of the polar vortex centroid—plays a more important role in the stratosphere-troposphere

coupling. Note that the influence of the changes in the zonal mean stratospheric winds on surface climate has been demonstrated in nudging experiments (e.g., Simpson et al., 2018); however, the potential impact of the latitudinal shift is less known.

Matsumura et al. (2021) also suggested that the zonal asymmetry in the stratospheric response can affect the surface climate response over Eurasia. We find that the relationship between the eastward polar vortex shift and surface climate is not significant in most cases except for  $\Delta U_{850}$  in SSP585. Instead, our results indicate that the surface temperature responses over Eurasia, the Pacific, and the western US are related to the changes in the strength and the latitudinal shift of the polar vortex whose direction, and therefore implications for the surface climate, are uncertain.

We conclude by emphasizing that the results of our paper show the potential to reduce climate projection uncertainty of the tropospheric circulation and hence regional surface climate change by narrowing the intermodel spread in projected stratospheric circulation changes. This, in turn, requires understanding the causes of the intermodel spread in projected stratospheric changes. A follow-up paper, currently in preparation, makes a step toward this goal by utilizing the data from the Dynamics and Variability Model Intercomparison Project (Gerber & Manzini, 2016) to explain the spread in terms of the stratospheric momentum budget, and to analyze potential drivers of the stratospheric response. Next to this analysis, more coordinated efforts by the modeling community are required to pinpoint the origins of the divergent circulation responses and to relate them to existing uncertainty in model representation of physical and dynamical processes. Such efforts may need to be prioritized when planning forthcoming CMIP experiments.

#### Acknowledgments

The authors acknowledge the World Climate Research Programme's Working Group on Coupled Modelling, which is responsible for CMIP, and the authors thank the climate modeling groups for producing and making available their model output. For CMIP, the U.S. Department of Energy's Program for Climate Model Diagnosis and Intercomparison provides coordinating support and led development of software infrastructure in partnership with the Global Organization for Earth System Science Portals. A.Y.K. was supported by the European Union's Horizon 2020 research and innovation framework programme under Grant agreement no. 101003590 (PolarRES). E.M. acknowledges the support of the German Federal Ministry of Education and Research through the JPI Climate/JPI Oceans NextG-Climate Science-ROADMAP (FKZ: 01LP2002A) project. M.K. has received funding from the European Union's Horizon 2020 research and innovation program under the Marie Skłodowska-Curie grant agreement (841902) and the NERC-funded project ArctiCONNECT (NE/V005855/1). H.A.-G. acknowledges funding from the European Union's Horizon 2020 research and innovation programme under the Marie Skłodowska-Curie grant agreement No 891514. Support from the Swiss National Science Foundation through project PP00P2\_198896 and PP00P2\_170523 to Z.W. and D.D. is gratefully acknowledged. The work of Z.W. is partially funded by the Swiss Data Science Center within the project EXPECT (C18-08). I.R.S. is supported by the National Center for Atmospheric Research, which is a major facility sponsored by the National Science Foundation under the Cooperative Agreement 1852977. A.H.B. and Z.D.L. were supported by the NOAA Climate Program Office's Modeling, Analysis, Predictions, and Projections program.

#### Data Availability Statement

CMIP5 and CMIP6 data are available from <https://esgf-node.llnl.gov/projects/esgf-llnl/>.

#### References

- Allen, R. J., & Sherwood, S. C. (2010). The impact of natural versus anthropogenic aerosols on atmospheric circulation in the Community Atmosphere Model. *Climate Dynamics*, 36(9–10), 1959–1978. <https://doi.org/10.1007/s00382-010-0898-8>
- Ayarzagüena, B., Charlton-Perez, A. J., Butler, A. H., Hitchcock, P., Simpson, I. R., Polvani, L. M., et al. (2020). Uncertainty in the response of sudden stratospheric warmings and stratosphere-troposphere coupling to quadrupled CO<sub>2</sub> concentrations in CMIP6 models. *Journal of Geophysical Research: Atmospheres*, 125(6), e2019JD032345. <https://doi.org/10.1029/2019JD032345>
- Ayarzagüena, B., Polvani, L. M., Langematz, U., Akiyoshi, H., Bekki, S., Butchart, N., et al. (2018). No robust evidence of future changes in major stratospheric sudden warmings: A multi-model assessment from CCM1. *Atmospheric Chemistry and Physics*, 18(15), 11277–11287. <https://doi.org/10.5194/acp-18-11277-2018>
- Barnes, E. A., & Polvani, L. M. (2013). Response of the midlatitude jets and of their variability to increased greenhouse gases in the CMIP5 models. *Journal of Climate*, 26(18), 7117–7135. <https://doi.org/10.1175/JCLI-D-12-00536.1>
- Butchart, N., & Remsberg, E. E. (1986). The area of the stratospheric polar vortex as a diagnostic for tracer transport on an isentropic surface. *Journal of the Atmospheric Sciences*, 43(13), 1319–1339. [https://doi.org/10.1175/1520-0469\(1986\)043<1319:TAOTSP>2.0.CO;2](https://doi.org/10.1175/1520-0469(1986)043<1319:TAOTSP>2.0.CO;2)
- Charlton-Perez, A. J., Baldwin, M. P., Birner, T., Black, R. X., Butler, A. H., Calvo, N., et al. (2013). On the lack of stratospheric dynamical variability in low-top versions of the CMIP5 models. *Journal of Geophysical Research: Atmospheres*, 118(6), 2494–2505. <https://doi.org/10.1002/jgrd.50125>
- Collins, M., Knutti, R., Arblaster, J., Dufresne, J.-L., Fichet, T., Friedlingstein, P., et al. (2013). Long-term climate change: Projections, commitments and irreversibility. In T. F. Stocker, D. Qin, G.-K. Plattner, M. Tignor, S. K. Allen, J. Boschung, et al. (Eds.), *Climate change 2013: The physical science basis. Contribution of working group I to the fifth assessment report of the intergovernmental panel on climate change*. Cambridge University Press.
- Dai, Y., & Hitchcock, P. (2021). Understanding the basin asymmetry in surface response to sudden stratospheric warmings from an ocean-atmosphere coupled perspective. *Journal of Climate*, 34(21), 8683–8698. <https://doi.org/10.1175/JCLI-D-21-0314.1>
- Garfinkel, C. I., Hartmann, D. L., & Sassi, F. (2010). Tropospheric precursors of anomalous Northern Hemisphere stratospheric polar vortices. *Journal of Climate*, 23(12), 3282–3299. <https://doi.org/10.1175/2010JCLI3010.1>
- Gerber, E. P., & Manzini, E. (2016). The dynamics and variability model intercomparison project (DynVarMIP) for CMIP6: Assessing the stratosphere-troposphere system. *Geoscientific Model Development*, 9, 3413–3425. <https://doi.org/10.5194/gmd-9-3413-2016>
- Hardiman, S. C., Butchart, N., Hinton, T. J., Osprey, S. M., & Gray, L. J. (2012). The effect of a well resolved stratosphere on surface climate: Differences between CMIP5 simulations with high and low top versions of the Met Office climate model. *Journal of Climate*, 25(20), 7083–7099. <https://doi.org/10.1175/JCLI-D-11-00579.1>
- Harvey, B. J., Cook, P., Shaffrey, L. C., & Schiemann, R. (2020). The response of the northern hemisphere storm tracks and jet streams to climate change in the CMIP3, CMIP5, and CMIP6 climate models. *Journal of Geophysical Research: Atmospheres*, 125(23), e2020JD032701. <https://doi.org/10.1029/2020JD032701>
- Hawkins, E., & Sutton, R. (2009). The potential to narrow uncertainty in regional climate predictions. *Bulletin of the American Meteorological Society*, 90(8), 1095–1107. <https://doi.org/10.1175/2009BAMS2607.1>
- Hitchcock, P., & Simpson, I. R. (2014). The downward influence of stratospheric sudden warmings. *Journal of the Atmospheric Sciences*, 71(10), 3856–3876. <https://doi.org/10.1175/JAS-D-14-0012.1>
- Karpechko, A. Y. (2010). Uncertainties in future climate attributable to uncertainties in future Northern Annular Mode trend. *Geophysical Research Letters*, 37(20), L20702. <https://doi.org/10.1029/2010GL044717>

- Karpechko, A. Y., & Manzini, E. (2012). Stratospheric influence on tropospheric climate change in the Northern Hemisphere. *Journal of Geophysical Research*, 117(D5), D05133. <https://doi.org/10.1029/2011JD017036>
- Karpechko, A. Y., & Manzini, E. (2017). Arctic stratosphere dynamical response to global warming. *Journal of Climate*, 30(17), 7071–7086. <https://doi.org/10.1175/JCLI-D-16-0781.1>
- Karpechko, A. Y., Maycock, A. C., Abalos, M., Akiyoshi, H., Arblaster, J. M., Garfinkel, C. I., et al. (2018). Stratospheric ozone changes and climate. In *Scientific assessment of ozone depletion: 2018* (pp. 44–46). World Meteorological Organization. Global Ozone Research and Monitoring Project Rep. 58.
- Karpechko, A., Kyrö, E., & Knudsen, B. M. (2005). Arctic and Antarctic polar vortices 1957–2002 as seen from the ERA-40 reanalyses. *Journal of Geophysical Research*, 110(D21), D21109. <https://doi.org/10.1029/2005JD006113>
- Kidston, J., Scaife, A. A., Hardiman, S. C., Mitchell, D. M., Butchart, N., Baldwin, M. P., & Gray, L. J. (2015). Stratospheric influence on tropospheric jet streams, storm tracks and surface weather. *Nature Geoscience*, 8(6), 433–440. <https://doi.org/10.1038/ngeo2424>
- Kretschmer, M., Zappa, G., & Shepherd, T. G. (2020). The role of Barents–Kara sea ice loss in projected polar vortex changes. *Weather Climate Dynamics*, 1(2), 715–730. <https://doi.org/10.5194/wcd-1-715-2020>
- Lehner, F., Deser, C., Maher, N., Marotzke, J., Fischer, E., Brunner, L., et al. (2020). Partitioning climate projection uncertainty with multiple large ensembles and CMIP5/6. *Earth System Dynamics*, 11(2), 491–508. <https://doi.org/10.5194/esd-11-491-2020>
- Levang, S. J., & Schmitt, R. W. (2015). Centennial changes of the global water cycle in CMIP5 models. *Journal of Climate*, 28(16), 6489–6502. <https://doi.org/10.1175/JCLI-D-15-0143.1>
- Manabe, S., & Wetherald, R. T. (1975). The effects of doubling the CO<sub>2</sub> concentration on the climate of a general circulation model. *Journal of the Atmospheric Sciences*, 32(1), 3–15. [https://doi.org/10.1175/1520-0469\(1975\)032<0003:teodtc>2.0.co;2](https://doi.org/10.1175/1520-0469(1975)032<0003:teodtc>2.0.co;2)
- Manzini, E., Karpechko, A. Y., Anstey, J., Baldwin, M. P., Black, R. X., Cagnazzo, C., et al. (2014). Northern winter climate change: Assessment of uncertainty in CMIP5 projections related to stratosphere troposphere coupling. *Journal of Geophysical Research: Atmospheres*, 119(13), 7979–7998. <https://doi.org/10.1002/2013JD021403>
- Manzini, E., Karpechko, A. Y., & Kornblueh, L. (2018). Nonlinear response of the stratosphere and the North Atlantic-European climate to global warming. *Geophysical Research Letters*, 45(9), 4255–4263. <https://doi.org/10.1029/2018GL077826>
- Matsumura, S., Yamazaki, K., & Horinouchi, T. (2021). Robust asymmetry of the future Arctic polar vortex is driven by tropical Pacific warming. *Geophysical Research Letters*, 48(11), e2021GL093440. <https://doi.org/10.1029/2021GL093440>
- Middlemas, E. A., Kay, J. E., Medeiros, B. M., & Maroon, E. A. (2020). Quantifying the influence of cloudradiative feedbacks on Arctic surfacewarming using cloud locking in an Earth system model. *Geophysical Research Letters*, 47(15), e2020GL089207. <https://doi.org/10.1029/2020GL089207>
- Mitchell, D. M., Charlton-Perez, A. J., & Gray, L. J. (2011). Characterizing the variability and extremes of the stratospheric polar vortices using 2D moment analysis. *Journal of the Atmospheric Sciences*, 68(6), 1194–1213. <https://doi.org/10.1175/2010jas3555.1>
- Mitchell, D. M., Osprey, S. M., Gray, L. J., Butchart, N., Hardiman, S. C., Charlton-Perez, A. J., & Watson, P. (2012). The effect of climate change on the variability of the Northern Hemisphere Stratospheric polar vortex. *Journal of the Atmospheric Sciences*, 69(8), 2608–2618. <https://doi.org/10.1175/jas-d-12-021.1>
- Oudar, T., Cattiaux, J., & Douville, H. (2020). Drivers of the northern extratropical eddy-driven jet change in CMIP5 and CMIP6 models. *Geophysical Research Letters*, 47(8), e2019GL086695. <https://doi.org/10.1029/2019GL086695>
- Pisof, P., Sacha, P., Polvani, L. M., Añel, J. A., De la Torre, L., Eichinger, R., et al. (2021). Stratospheric contraction caused by increasing greenhouse gases. *Environmental Research Letters*, 16(2021), 064038. <https://doi.org/10.1088/1748-9326/abfe2b>
- Rao, J., & Garfinkel, C. I. (2021). CMIP5/6 models project little change in the statistical characteristics of sudden stratospheric warmings in the 21st century. *Environmental Research Letters*, 16(3), 034024. <https://doi.org/10.1088/1748-9326/abd4fe>
- Rao, J., Garfinkel, C. I., Wu, T., Lu, Y., & Chu, M. (2022). Mean state of the northern hemisphere stratospheric polar vortex in three generations of CMIP models. *Journal of Climate*, 35(14), 4603–4625. <https://doi.org/10.1175/JCLI-D-21-0694.1>
- Reichler, T., Kim, J., Manzini, E., & Kröger, J. (2012). A stratospheric connection to Atlantic climate variability. *Nature Geoscience*, 5(11), 783–787. <https://doi.org/10.1038/ngeo1586>
- Scaife, A. A., Spanghel, T., Fereday, D. R., Cubasch, U., Langematz, U., Akiyoshi, H., et al. (2012). Climate change projections and stratosphere-troposphere interaction. *Climate Dynamics*, 38(9–10), 2089–2098. <https://doi.org/10.1007/s00382-011-1080-7>
- Seviour, W. J. M., Mitchell, D. M., & Gray, L. J. (2013). A practical method to identify displaced and split stratospheric polar vortex events. *Geophysical Research Letters*, 40(19), 5268–5273. <https://doi.org/10.1002/grl.50927>
- Shepherd, T. G. (2014). Atmospheric circulation as a source of uncertainty in climate change projections. *Nature Geoscience*, 7(10), 703–708. <https://doi.org/10.1038/ngeo2253>
- Shepherd, T. G., & McLandress, C. (2011). A robust mechanism for strengthening of the Brewer–Dobson circulation in response to climate change: Critical-layer control of subtropical wave breaking. *Journal of the Atmospheric Sciences*, 68(4), 784–797. <https://doi.org/10.1175/2010JAS3608.1>
- Shindell, D. T., Miller, R. L., Schmidt, G. A., & Pandolfo, L. (1999). Simulation of recent northern winter climate trends by greenhouse-gas forcing. *Nature*, 399(6735), 452–455. <https://doi.org/10.1038/20905>
- Sigmond, M., & Scinocca, J. F. (2010). The influence of the basic state on the Northern Hemisphere circulation response to climate change. *Journal of Climate*, 23(6), 1434–1446. <https://doi.org/10.1175/2009JCLI3167.1>
- Sigmond, M., Siegmund, P. C., Manzini, E., & Kelder, H. (2004). A simulation of the separate climate effects of middle atmospheric and tropospheric CO<sub>2</sub> doubling. *Journal of Climate*, 17(12), 2352–2367. [https://doi.org/10.1175/1520-0442\(2004\)017<2352:ASOTSC>2.0.CO;2](https://doi.org/10.1175/1520-0442(2004)017<2352:ASOTSC>2.0.CO;2)
- Simpson, I. R., Hitchcock, P., Seager, R., Wu, Y., & Callaghan, P. (2018). The downward influence of uncertainty in the Northern Hemisphere stratospheric polar vortex response to climate change. *Journal of Climate*, 31(16), 6371–6391. <https://doi.org/10.1175/JCLI-D-18-0041.1>
- Smith, D. M., Eade, R., Andrews, M. B., Ayres, H., Clark, A., Chripko, S., et al. (2022). Robust but weak winter atmospheric circulation response to future Arctic sea ice loss. *Nature Communications*, 13(1), 727. <https://doi.org/10.1038/s41467-022-28283-y>
- Stephenson, D. B., & Held, I. M. (1993). GCM response of northern winter stationary waves and storm tracks to increasing amounts of carbon dioxide. *Journal of Climate*, 6(10), 1859–1870. [https://doi.org/10.1175/1520-0442\(1993\)006<1859:gronws>2.0.co;2](https://doi.org/10.1175/1520-0442(1993)006<1859:gronws>2.0.co;2)
- Sun, L., Deser, C., & Tomas, R. A. (2015). Mechanisms of stratospheric and tropospheric circulation response to projected Arctic Sea ice loss. *Journal of Climate*, 28(19), 7824–7845. <https://doi.org/10.1175/JCLI-D-15-0169.1>
- Waugh, D. N. W. (1997). Elliptical diagnostics of stratospheric polar vortices. *Quarterly Journal of the Royal Meteorological Society*, 123(542), 1725–1748. <https://doi.org/10.1002/qj.49712354213>
- Wilks, D. S. (2016). The stippling shows statistically significant grid points: How research results are routinely overstated and overinterpreted, and what to do about it. *Bulletin of the American Meteorological Society*, 97(12), 2263–2273. <https://doi.org/10.1175/BAMS-D-15-00267.1>

- Woollings, T. (2008). Vertical structure of anthropogenic zonal-mean atmospheric circulation change. *Geophysical Research Letters*, 35(19), L19702. <https://doi.org/10.1029/2008GL034883>
- Woollings, T., & Blackburn, M. (2012). The North Atlantic jet stream under climate change and its relation to the NAO and EA patterns. *Journal of Climate*, 25(3), 886–902. <https://doi.org/10.1175/jcli-d-11-00087.1>
- Wu, Y., Simpson, I. R., & Seager, R. (2019). Intermodel spread in the northern hemisphere stratospheric polar vortex response to climate change in the CMIP5 models. *Geophysical Research Letters*, 46(22), 13290–13298. <https://doi.org/10.1029/2019GL085545>
- Yip, S., Ferro, C. A. T., Stephenson, D. B., & Hawkins, E. (2011). A simple, coherent framework for partitioning uncertainty in climate predictions. *Journal of Climate*, 24(17), 4634–4643. <https://doi.org/10.1175/2011JCLI4085.1>
- Zappa, G., & Shepherd, T. G. (2017). Storylines of atmospheric circulation change for European regional climate impact assessment. *Journal of Climate*, 30(16), 6561–6577. <https://doi.org/10.1175/JCLI-D-16-0807.1>